RESEARCH ARTICLE

WILEY

Structural connectivity of autonomic, pain, limbic, and sensory brainstem nuclei in living humans based on 7 Tesla and 3 Tesla MRI

Kavita Singh[1] ![] | María Guadalupe García-Gomar[1,2] ![] | Simone Cauzzo[1,3,4] |
Jeffrey P. Staab[5,6] | Iole Indovina[7,8] | Marta Bianciardi[1,9]

[1]Brainstem Imaging Laboratory, Department of Radiology, Athinoula A. Martinos Center for Biomedical Imaging, Massachusetts General Hospital and Harvard Medical School, Boston, Massachusetts, USA

[2]Escuela Nacional de Estudios Superiores, Juriquilla, Universidad Nacional Autónoma de México, Querétaro, Mexico

[3]Life Sciences Institute, Sant'Anna School of Advanced Studies, Pisa, Italy

[4]Research Center E. Piaggio, University of Pisa, Pisa, Italy

[5]Department of Psychiatry and Psychology, Mayo Clinic, Rochester, Minnesota, USA

[6]Department of Otorhinolaryngology – Head and Neck Surgery, Mayo Clinic, Rochester, Minnesota, USA

[7]Department of Biomedical and Dental Sciences and Morphofunctional Imaging, University of Messina, Italy

[8]Laboratory of Neuromotor Physiology, IRCCS Santa Lucia Foundation, Rome, Italy

[9]Division of Sleep Medicine, Harvard University, Boston, Massachusetts, USA

Correspondence
Kavita Singh and Marta Bianciardi, Department of Radiology, Athinoula A. Martinos Center for Biomedical Imaging, Massachusetts General Hospital and Harvard Medical School, Building 149, Room 2301, 13th Street, Charlestown, Boston, MA 02129, USA.
Email: ksingh0@mgh.harvard.edu and martab@mgh.harvard.edu

Abstract

Autonomic, pain, limbic, and sensory processes are mainly governed by the central nervous system, with brainstem nuclei as relay centers for these crucial functions. Yet, the structural connectivity of brainstem nuclei in living humans remains understudied. These tiny structures are difficult to locate using conventional in vivo MRI, and ex vivo brainstem nuclei atlases lack precise and automatic transformability to in vivo images. To fill this gap, we mapped our recently developed probabilistic brainstem nuclei atlas developed in living humans to high-spatial resolution (1.7 mm isotropic) and diffusion weighted imaging (DWI) at 7 Tesla in 20 healthy participants. To demonstrate clinical translatability, we also acquired 3 Tesla DWI with conventional resolution (2.5 mm isotropic) in the same participants. Results showed the structural connectome of 15 autonomic, pain, limbic, and sensory (including vestibular) brainstem nuclei/nuclei complex (superior/inferior colliculi, ventral tegmental area-parabrachial pigmented, microcellular tegmental–parabigeminal, lateral/medial parabrachial, vestibular, superior olivary, superior/inferior medullary reticular formation, viscerosensory motor, raphe magnus/pallidus/obscurus, parvicellular reticular nucleus-alpha part), derived from probabilistic tractography computation. Through

Kavita Singh and María Guadalupe García-Gomar equally contributed to this work and share first authorship.

graph measure analysis, we identified network hubs and demonstrated high inter-community communication in these nuclei. We found good ($r = .5$) translational capability of the 7 Tesla connectome to clinical (i.e., 3 Tesla) datasets. Furthermore, we validated the structural connectome by building diagrams of autonomic/pain/limbic connectivity, vestibular connectivity, and their interactions, and by inspecting the presence of specific links based on human and animal literature. These findings offer a baseline for studies of these brainstem nuclei and their functions in health and disease, including autonomic dysfunction, chronic pain, psychiatric, and vestibular disorders.

KEYWORDS
7 Tesla MRI, autonomic/pain/limbic/sensory network, brainstem, human structural connectome

1 | INTRODUCTION

Autonomic, pain, limbic and sensory functions in the body are mainly governed by networks from the brainstem-to-cortex involving brainstem nuclei such as the ventral tegmental area-parabrachial pigmented nucleus complex (VTA-PBP; G. Holstege et al., 2003; Ikemoto & Wise, 2004), microcellular tegmental–parabigeminal nucleus (MiTg-PBG; Usunoff, Schmitt, Itzev, Rolfs, & Wree, 2007), lateral parabrachial nucleus (LPB), medial parabrachial nucleus (MPB; Kaur et al., 2017; Veening, Swanson, & Sawchenko, 1984), parvicellular reticular nucleus-alpha part (PCRtA; Dessem & Luo, 1999), superior medullary reticular formation (sMRt; Robinson, Phillips, & Fuchs, 1994), inferior medullary reticular formation (iMRt; García-Gomar, Videnovic, et al., 2021), raphe magnus (RMg; Hornung, 2003), raphe obscurus (ROb; Nieuwenhuys, Voogd, & Van Huijzen, 2008), raphe pallidus (RPa; Hornung, 2003; Loewy & Neil, 1981), viscerosensory motor nuclei complex (VSM; Chamberlin & Saper, 1995; Nieuwenhuys et al., 2008), superior colliculus (SC; Lee & Groh, 2012; May, 2006), inferior colliculus (IC; Aitkin, 1979), vestibular nuclei complex (Ve; Goldberg et al., 2012), and superior olivary complex (SOC; Fay, Popper, & Webster, 1992). These nuclei with their overlapping functional domains provide a network of connectivity modulating respiration, cardiac function, initial processing of sensory stimuli including pain, metabolic control including thermoregulation, memory storage, and sexual arousal, integrated with reflexive emotional responses (Hermann, Luppi, Peyron, Hinckel, & Jouvet, 1997; Morgane, Galler, & Mokler, 2005; Schmidt, 1989; Uschakov, Gong, McGinty, & Szymusiak, 2007).

Despite their involvement in these critical functions, the study of their structural connectivity in living humans remains sparse (Englot et al., 2018; Harper, Kumar, Ogren, & Macey, 2013; Reisert, Weiller, & Hosp, 2021; C. Wang, Laiwalla, Salamon, Ellingson, & Holly, 2020; Wirth, Frank, Greenlee, & Beer, 2018). Brainstem nuclei are difficult to locate in living human participants using clinical neuroimaging technologies. Postmortem human atlases (J. Olszewski & Baxter, 1954; Paxinos & Huang, 1995; Paxinos, Xu-Feng, Sengul, & Watson, 2012) lack the precision and automatic transformability onto clinical images

for such investigations. Moreover, it is unclear to which extent high-contrast and high-spatial resolution diffusion-weighted imaging is needed to study their structural connectivity and build a map in living humans called a "structural connectome" or if conventional imaging will suffice.

To this end we utilized our recently developed atlas of brainstem nuclei (Bianciardi et al., 2018, 2016; García-Gomar et al., 2019; García-Gomar, Videnovic, et al., 2021; Singh, García-Gomar, & Bianciardi, 2021; Singh et al., 2019, 2021), released within the Brainstem Navigator toolkit (https://www.nitrc.org/projects/brainstemnavig/) and achieved using multicontrast and high-spatial resolution images at 7 Tesla in living humans, to generate a comprehensive structural connectome of autonomic, pain, limbic, and sensory nuclei. To do so, we mapped this atlas to high-spatial resolution (1.7 mm isotropic) diffusion weighted imaging (DWI) at 7 Tesla on 20 healthy participants. To create a comprehensive form of the connectome that can be translated to clinical datasets, we also acquired 3 Tesla DWI with conventional (2.5 mm isotropic) resolution in the same participants and compared the structural connectome obtained at 3 Tesla with the connectome obtained at 7 Tesla.

To validate our structural connectome of brainstem nuclei, we inspected our results from a system neuroscience perspective, based on the structural connectivity and interactions of autonomic, pain, somatosensory, and vestibular pathways detailed in neuroanatomical and neurophysiological studies in humans and animals.

2 | METHODS

2.1 | Data acquisition

A total of 20 healthy participants (10 males and 10 females; mean ± *SE* age 29.5 ± 1.1 years) underwent 7 Tesla (Magnetom; Siemens Healthineers) and 3 Tesla (Connectom; Siemens Healthineers) MRI after giving written informed consent for the study. One participant was excluded due to poor image quality. In the excluded subject, in the S_0 image, midbrain and thalamus showed decreased sensitivity

compared to the other subjects; moreover, brainstem region showed signal drop out and increased spatial distortions in anterior pons due to increased field inhomogeneities, as well as decreased glyph amplitude of the fiber orientation distribution (FOD) function. Thus, only 19 participants were included in the study cohort (10 males and 9 females; mean ± SE age 29.0 ± 5 years). This study protocol was approved by Institutional Review Board at the Massachusetts General Hospital. We randomized the session order across participants. To focus on translatability to typical clinical settings, we used a conventional diffusion-weighted sequence at 3 Tesla, and we did not employ the 3 Tesla Connectom capabilities of the scanner. During both 7 Tesla and 3 Tesla MRI acquisition sessions, participants were asked to lie supine in the scanner remaining as still as possible assisted with foam pads placed beneath their neck to minimize head movements. At 7 Tesla, we used a custom-built 32-channel receive coil and volume transmit coil, providing enhanced sensitivity in the deeper brainstem regions than commercial coils. For 3 Tesla we used 64-channel receive coil and volume transmit coil (Keil et al., 2013).

2.1.1 | 7 Tesla MRI data acquisition

To acquire high-spatial resolution (1.7 mm isotropic) DWI data, we used common single-shot 2D spin-echo echo-planar images (EPI; using a prototype sequence which supports unipolar diffusion encoding) with the following parameters: number of slices = 82, echo time = 66.8 ms repetition time = 7.4 s, phase encoding direction = anterior/posterior, bandwidth = 1,456 Hz/pixel, partial Fourier = 6/8, number of diffusion directions = 60, b value = 2,500-s/mm^2, acquisition time = 8′53″. To perform distortion correction, we also acquired 7 "b0" images (b value $\sim$0 s/mm^2) with opposite phase-encoding direction. Non-diffusion-weighted EPIs of the DWI protocol were used as T_2-weighted images with matched geometric distortions and spatial resolution to the DWI images. The use of T_2-weighted EPIs also allowed to overcome specific absorption rate limits usually encountered with spin-warp T_2-weighted MRI at ultrahigh magnetic field.

2.1.2 | 3 Tesla MRI data acquisition

To access clinical translatability of our structural connectome, we acquired DWI images on the same participants participating to the 7 Tesla MRI session with conventional spatial resolution (2.5 mm isotropic) and with the following parameters: number of slices = 64, echo time = 84 ms, repetition time = 7,300 ms, phase encoding direction = anterior/posterior, bandwidth = 2,422 Hz/pixel, partial Fourier = 7/8, number of diffusion directions = 60, b value = 2,500-s/mm^2, acquisition time = 9′29″. To perform distortion correction we also acquired 8 "b0" images with opposite phase-encoding direction. Non-diffusion-weighted EPIs of the DWI protocol were used as T_2-weighted images with matched geometric distortions and spatial resolution to the DWI images.

During the 3 Tesla MRI session, to define cortical and subcortical target regions, we also acquired an anatomical T_1-weighted MEMPRAGE image with isotropic voxel size = 1 mm, repetition time = 2.53 s, echo times = 1.69, 3.5, 5.3, 7.2 ms, inversion time = 1.5 s, flip angle = 7°, FOV = 256 × 256 × 176 mm^3, bandwidth = 650 Hz/pixel, GRAPPA factor = 3, slice orientation = sagittal, slice-acquisition order = anterior–posterior acquisition time = 4′28″.

2.2 | Data processing

2.2.1 | MEMPRAGE processing

For each participant, we computed the root-mean-square of the MEMPRAGE image across echo times. We then rotated it to standard orientation ("RPI"), bias field corrected (SPM; Frackowiak, Ashburner, Penny, & Zeki, 2004), brain extracted and cropped the lower slices (*FSL 5.0.7 tools-FMRIB Software Library, FSL, Oxford, UK*). The preprocessed MEMPRAGE was parcellated with Freesurfer (Destrieux, Fischl, Dale, & Halgren, 2010) to generate cortical and subcortical targets. These parcellations were registered to S_0 native space via FLIRT boundary-based affine registration (FSL).

2.2.2 | 7 Tesla diffusion data analysis

DWI images were denoised (Manjón et al., 2013), motion and distortion corrected (FSL, topup/eddy). The diffusion tensor was computed (FSL, dtifit), yielding diffusion tensor invariants such as the diffusion fractional anisotropy (FA), as well as the non-diffusion-weighted S_0 signal, carrying the T_2-weighted MRI signal component. To map the Freesurfer parcellation to native DWI-space, we computed an affine boundary-based transformation (FSL, FLIRT-BBR) between the preprocessed MEMPRAGE and single-participant S_0. To map the brainstem nuclei atlas from Illinois Institute of Technology (IIT) MNI (IIT-MNI) space to native DWI-space, we built an optimal template from the FA/S_0 images of 20 participants using the Advanced Normalization Tool (ANTs). The optimal template was then registered to the IIT-MNI FA/S_0 templates (Grabner et al., 2006) through an affine transformation and a nonlinear warp. Finally, we combined the transformation matrices from single participants' FA/S_0 to the optimal template and from the optimal template to IIT-MNI FA/S_0 templates to obtain the full coregistration matrix, which aligned the labels from IIT-MNI space to single-participant DWI-space.

For tract generation, we performed probabilistic tractography using MRtrix3 software package (http://www.mrtrix.org; Tournier, Calamante, & Connelly, 2012). Using dwi2response (with the "tournier" algorithm; Tournier, Calamante, & Connelly, 2013), we estimated response functions from the preprocessed diffusion-weighted images. These were then used to estimate FOD based on constrained spherical deconvolution using dwi2fod (Tournier, Calamante, & Connelly, 2007). For fiber tracking, we then used tckgen with the

improved second-order integration over fiber orientation distributions (iFOD2) algorithm (Tournier, Calamante, & Connelly, 2010). The following tckgen settings with the following parameters were used: desired number of streamlines = 100,000, maximum angle between successive steps = 90°, minimum streamline length = 1 mm, FOD amplitude cut-off = 0.07. We computed a "structural connectivity index" (range: [0 1]) for each pair of seed target masks (number of streamlines propagated from the seed reaching the target mask divided by 100,000). For each participant, the structural connectivity index was arranged in a connectivity matrix (size: number of seeds × number of targets). We ran a one sample Kolmogorov–Smirnov test for normality across participants. Since the connectivity indices did not follow a normal distribution across participants, we ran a Wilcoxon signed-rank test, followed by false discovery rate (FDR) correction for multiple comparisons. An FDR corrected threshold of .0005 was used, and significant values for all the seeds were displayed as a matrix and as a 2D circular diagram (i.e., "2D-connectome"; Irimia, Chambers, Torgerson, & Van Horn, 2012). For single seeds also, a 2D circular diagram was displayed. For each seed, tracts were converted to nifti format (nonbinarized; tckmap in MRtrix), registered to IIT space and averaged across participants (fslmaths). Wilcoxon signed-rank test (Matlab) was computed for each seed and displayed as mean tract density map.

## 2.3 | Defining seed and target regions for 2D connectome generation

For the 2D connectome generation described above, a probabilistic atlas of brainstem nuclei developed by our group (Bianciardi et al., 2018, 2016; García-Gomar, Singh, & Bianciardi, 2021; García-Gomar et al., 2019; Singh et al., 2019, 2021), recently released within the Brainstem Navigator toolkit (https://www.nitrc.org/projects/brainstemnav/), and FreeSurfer cortical and subcortical parcellation (Destrieux et al., 2010) were used to define seed and target regions. Specifically, we used as seed regions the probabilistic atlas labels (binarized by setting a threshold at 35%) of the following 15 brainstem nuclei (https://www.nitrc.org/projects/brainstemnav/; Bianciardi et al., 2018, 2016; García-Gomar et al., 2019; García-Gomar, Videnovic, et al., 2021; Singh et al., 2021, 2019; 12 bilateral and 3 midline nuclei, for a total of 27 nuclei) involved in autonomic, limbic, pain, and sensory processing: RMg, LPB, MPB, VTA-PBP, RPa, ROb, VSM, sMRt, iMRt, PCRtA, Ve, SC, IC, SOC, and MiTg-PBG.

We defined as target regions the 27 autonomic/limbic/pain/sensory seed regions defined above, and 18 (31 counting bilateral nuclei) probabilistic atlas labels (binarized by setting a threshold at 35%) of brainstem nuclei (https://www.nitrc.org/projects/brainstemnav/; Bianciardi et al., 2018, 2016; García-Gomar et al., 2019; García-Gomar, Videnovic, et al., 2021; Singh et al., 2021, 2019), involved in wakeful arousal and motor function (Datta, Curró Dossi, Paré, Oakson, & Steriade, 1991; Lima, Andersen, Reksidler, Vital, & Tufik, 2007; Lima, Reksidler, & Vital, 2008; Merel, Botvinick, & Wayne, 2019; Moruzzi & Magoun, 1949; J. Olszewski & Baxter, 1954; Parvizi & Damasio, 2001; Saper, Chou, & Scammell, 2001; Saper, Fuller, Pedersen, Lu, & Scammell, 2010), namely, median raphe (MnR), paramedian raphe (PMnR), and dorsal raphe (DR); substantia nigra-subregion1 (SN1; compatible with pars reticulata), and substantia nigra-subregion2 (SN2; compatible with pars compacta), caudal–rostral linear raphe (CLi-RLi), periaqueductal gray (PAG); mesopontine reticular formation nuclei: mesencephalic reticular formation (mRt), cuneiform nucleus (CnF), isthmic reticular formation (isRt), and pontine reticular formation oral and caudal part (PnO-PnC); noradrenergic nucleus of locus coeruleus (LC), and subcoeruleus (SubC), (J. Olszewski & Baxter, 1954; Parvizi & Damasio, 2001; Saper et al., 2001, 2010); cholinergic pedunculotegmental nucleus (PTg) and laterodorsal tegmental nucleus–central gray of the rhombencephalon (LDTg-CGPn); nuclei mainly involved in motor function red nucleus-subregion1 (RN1), red nucleus-subregion2 (RN2), and inferior olivary nucleus (ION). In addition, we used as target regions, 74 FreeSurfer bilateral cortical (Destrieux et al., 2010) and 9 bilateral single-subject parcellations (described above in Section 2.2.1) including cerebellar cortex, caudate, putamen, pallidum, amygdala, hippocampus, thalamus, subthalamic nucleus subregion1, and 2 (Bianciardi et al., 2015), and hypothalamus (Pauli, Nili, & Tyszka, 2018). We also used as target the basal forebrain region, including the accumbens (Desikan et al., 2006), substantia innominata and diagonal band of Broca (Snider et al., 2019). Descriptive list of seeds and targets is shown in Figure 1. Moreover, in Table 1 we list all brainstem seeds and targets, as well as their function. In Tables S1 and S2 we provide a comprehensive list of all non-brainstem targets.

2.4 | Graph analysis

Graph analysis metrics were computed using the GRETNA (GRaph thEoreTical Network Analysis) Matlab toolbox (http://www.nitrc.org/projects/gretna/; J. Wang et al., 2015) on a square matrix obtained by setting to zero the non-seeds to targets connectivity values (note that computation of these values was beyond the scope of this work, and would require extensive computation). For each seed region, we extracted only the nodal measures (degree centrality, and normalized participant coefficient) unaffected by non-seed to target connectivity values (here set to zero), as expected from graph theory (Rubinov, Sporns, van Leeuwen, & Breakspear, 2009). Other nodal measures, such as betweenness centrality, local efficiency, clustering coefficient, and shortest path length instead depend (Rubinov et al., 2009) on these values, and thus were not computed. Degree centrality is defined as the number of edges connected to a node, is an extensively adopted measure used to quantify the hubness of each node, and has a direct neurobiological interpretation (Bullmore & Sporns, 2009; Rubinov & Sporns, 2010). Normalized participant coefficient reflects the ability of a node in keeping communication between its own module and the other modules, scaled by the maximum of this measure across all nodes. To compute the normalized participant coefficient,
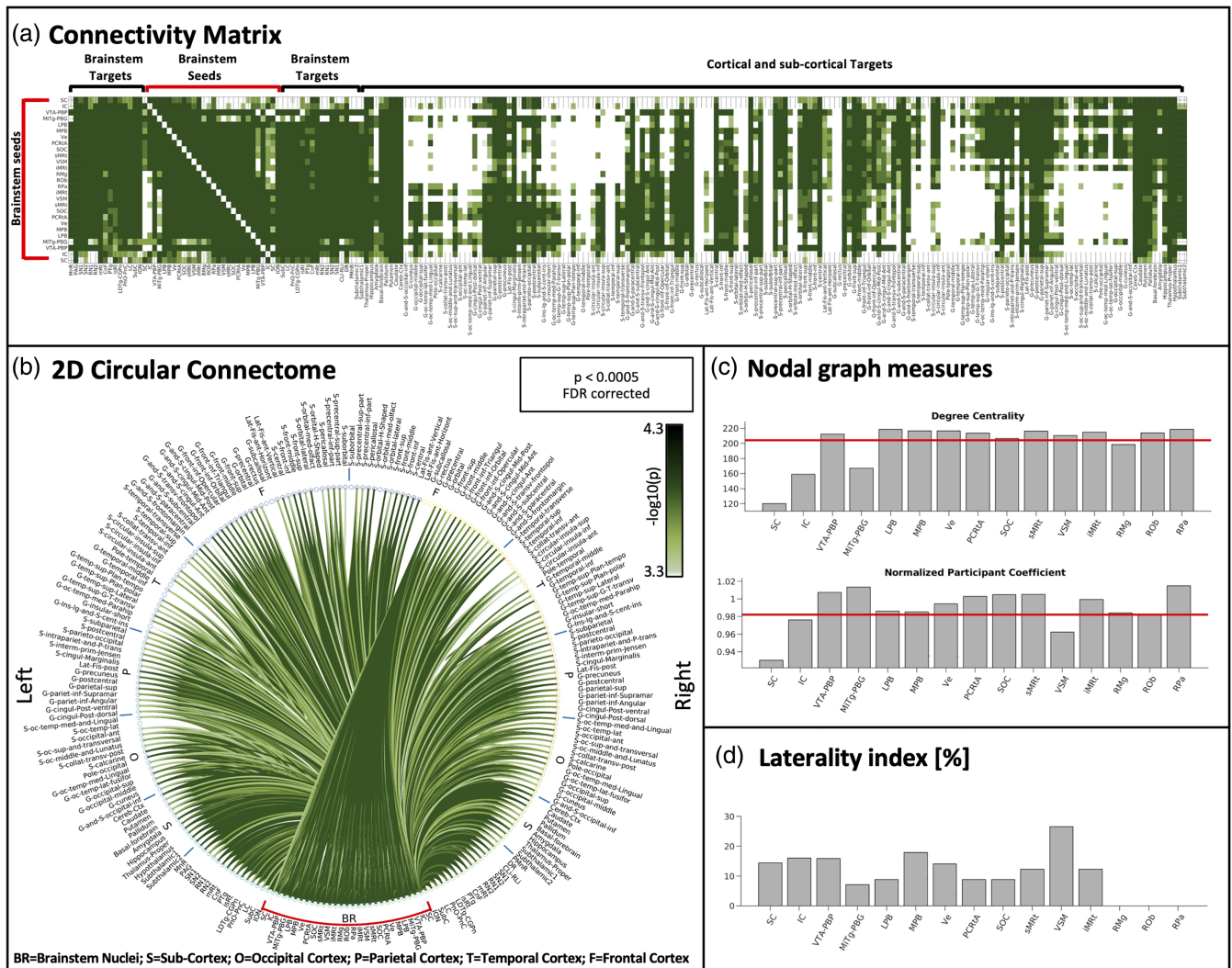
FIGURE 1 Connectivity matrix, 2D circular connectome, nodal graph measures and laterality index of all autonomic, pain, limbic and sensory brainstem nuclei. (a) The 2D connectivity matrix, (b) the region-based 2D structural connectome at the group level of the autonomic, pain, limbic, and sensory brainstem nuclei (for both a and b we used a $p < .0005$ false discovery rate (FDR) corrected threshold and display the ($-\log_{10}(p$ value)). (c) We display nodal graph measures (such as degree centrality and normalized participant coefficient) and (d) the laterality index. List of abbreviations of 15 brainstem nuclei used as seeds (marked with red brackets in a and b): superior colliculus (SC), inferior colliculus (IC), ventral tegmental area-parabrachial pigmented nucleus (VTA-PBP), microcellular tegmental nucleus–parabigeminal nucleus (MiTg-PBG), lateral parabrachial nucleus (LPB), medial parabrachial nucleus (MPB), vestibular nuclei complex (Ve), parvicellular reticular nucleus-alpha part (PCRtA), superior olivary complex (SOC), superior medullary reticular formation (sMRt), viscerosensory motor nuclei complex (VSM), inferior medullary reticular formation (iMRt), raphe magnus (RMg), raphe obscurus (ROb) and raphe pallidus (RPa). List of abbreviations of 18 additional brainstem nuclei used as targets: median raphe nucleus (MnR), periaqueductal gray (PAG), substantia nigra-subregion1 (SN1), substantia nigra-subregion2 (SN2), red nucleus-subregion1 (RN1), red nucleus-subregion2 (RN2), mesencephalic reticular formation (mRt), cuneiform nucleus (CnF), pedunculotegmental nucleus (PTg), isthmic reticular formation (isRt), laterodorsal tegmental nucleus–central gray of the rhombencephalon (LDTg-CGPn), pontine reticular nucleus, oral part–pontine reticular nucleus, caudal part (PnO-PnC), locus coeruleus (LC), subcoeruleus nucleus (SubC), inferior olivary nucleus (ION), caudal–rostral linear raphe (CLi-RLi), dorsal raphe (DR), and paramedian raphe nucleus (PMnR)

the network was divided into seven communities (seeds, brainstem targets, subcortical targets, occipital, temporal, frontal, and parietal cortical targets). Finally, for each bilateral seed, we computed (in Matlab) a laterality index defined as the difference between the binarized connectome of the left seed and the mirrored binarized connectome of the right seed, divided by the number of active links, thus scoring 0% for perfectly symmetric connectivity and 100% for perfectly asymmetric one.

2.5 | 3 Tesla diffusion data processing and correlation-analysis between 3 Tesla and 7 Tesla DTI datasets

Diffusion data acquired on the 3 Tesla scanner underwent a processing pipeline similar to 7 Tesla diffusion data. To access the translatability of our 7 Tesla connectome data with conventional data acquired at 3 Tesla, we computed the correlation coefficient between

TABLE 1 List of investigated brainstem nuclei used as seeds and targets, and their involvement in different functions

	Brainstem nuclei	Function	
	Seeds	**Autonomic, pain, limbic**	**Sensory**
1	Superior colliculus (SC)[a]		x
2	Inferior colliculus (IC)		x
3	Ventral tegmental area-parabrachial pigmented nucleus (VTA-PBP)[b]	x	
4	Microcellular tegmental nucleus–parabigeminal nucleus (Mitg-PBG)		x
5	Lateral parabrachial nucleus (LPB)[b]	x	x
6	Medial parabrachial nucleus (MPB)	x	x
7	Vestibular nuclei complex (Ve)[a,b]		x
8	Parvocellular reticular nucleus alpha part (PCRtA)[a]	x	
9	Superior olivary complex (SOC)		x
10	Superior medullary reticular formation (sMRt)[a]	x	
11	Viscerosensory motor nuclei complex (VSM)[a]	x	
12	Inferior medullary reticular formation (iMRt)[a]	x	
13	Raphe magnus (RMg)	x	
14	Raphe obscurus (ROb)[a]	x	
15	Raphe pallidus (RPa)[a]	x	
	Targets	**Arousal**	**Motor**
1	Median raphe nucleus (MnR)	x	
2	Periaqueductal gray (PAG)[c]	x	
3	Substantia nigra-subregion1 (SN1)	x	x
4	Substantia nigra-subregion2 (SN2)	x	x
5	Red nucleus-subregion1 (RN1)		x
6	Red nucleus-subregion2 (RN2)		x
7	Mesencephalic reticular formation (mRt)	x	x
8	Cuneiform (CnF)	x	x
9	Pedunculotegmental nuclei (PTg)	x	x
10	Isthmic reticular formation (isRt)	x	x
11	Laterodorsal tegmental nucleus–central Gray of the rhombencephalon (LDTg-CGPn)	x	
12	Pontine reticular nucleus, oral part–pontine reticular nucleus, caudal part (PnO-PnC)	x	x
13	Locus coeruleus (LC)[c]	x	
14	Subcoeruleus nucleus (SubC)		x
15	Inferior olivary nucleus (ION)		x
16	Caudal–rostral linear raphe (CLi-RLi)[c]	x	
17	Dorsal raphe (DR)[c,d]	x	
18	Paramedian raphe nucleus (PMnR)	x	

[a]Also involved in motor function.
[b]Also involved in arousal.
[c]Also involved in autonomic, pain, limbic function.
[d]Also involved in sensory function.

the two structural connectivity indices matrices (3 Tesla vs. 7 Tesla), averaged across participants. Percentage of common links across the two scanners for different statistical thresholds were computed. Significance of the correlation was assessed in all cases at $p < .05$ FDR corrected. Robustness of data were measured at different threshold values.

2.6 | Diagram generation

We explored functional circuits of the autonomic/limbic/nociceptive system, the vestibular sensory circuit, and their interactions. For these circuits, we used as nodes the brainstem nuclei and cortical macro-regions (based on clinical and preclinical studies; Balaban, 2004;

Indovina et al., 2020; Lacalle & Saper, 2000; Saper & Stornetta, 2015; Yasui, Saper, & Cechetto, 1989), and connectivity values of our human structural connectome as the links. Specifically, we averaged the connectivity strength of subregions belonging to a same node and, for each node, of left and right values, to yield a single connectivity value among nodes. We used solid lines to depict brainstem-to-brain links and varied the line thickness of each link based on the connectivity significance. A threshold of $p < .0005$ FDR corrected was used to assess the significance of connections. To generate the circuit diagram, we expanded the list of current targets to add more regions relating to similar functions being studied based on FreeSurfer parcellation (Destrieux et al., 2010). However, FreeSurfer parcellation does not include smaller regions such as fastigial nuclei (Fan et al., 2016), visual-motion cortex (including regions V5/MT+ region; Fan et al., 2016), and posterior insula (including areas Ig1 and Ig2; Fan et al., 2016), which we wanted to explore to provide a summary and more detailed diagram of vestibular, autonomic circuits and of their interaction. Thus we also used a combination of the Eickhoff (Eickhoff et al., 2005) and Fan (Fan et al., 2016) atlases in MNI space as described in (Indovina et al., 2020; the two atlases where unified and where two regions from the two atlases partially overlapped, two distinct regions were defined after subtracting the overlap area, one by selecting the Eickhoff area (Eickhoff et al., 2005) and one by selecting the Brainnetome area (Fan et al., 2016). We coregistered, these atlas labels from MNI space to native space by combining the transformation matrices from (i) MNI to IIT space (computed in Bianciardi et al., 2015) and (ii) IIT to native space via optimal template (as explained in Section 2.2.2).

Specifically, *for the autonomic/limbic/pain circuit*, we added three regions from FreeSurfer parcellation namely, (1) infralimbic cortex, defined as the macroregion containing rectus gyrus and subcallosal gyrus; (2) orbitofrontal cortex, including the orbital part of the inferior frontal gyrus, orbital gyrus, horizontal ramus and vertical ramus of the anterior segment of the lateral sulcus, lateral orbital sulcus, medial orbital (olfactory) sulcus, orbital h-shaped sulcus and suborbital sulcus; (3) anterior cingulate cortex with anterior and middle-anterior parts of the cingulate gyrus and sulcus; and two regions from Eickhoff–Fan atlas (Eickhoff et al., 2005; Fan et al., 2016), namely, (4) anterior insula, including dorsal agranular insula, ventral agranular insula and temporal agranular insular cortex; (5) fastigii nuclei. In the *vestibular circuit*, we added the following regions from Eickhoff and Fan parcellation: (5) fastigii nuclei (Eickhoff et al., 2005); (6) cerebellar lobule X (Eickhoff et al., 2005); (7) intraparietal sulcus, including areas hIP1, hIP2, and hIP3 (Eickhoff et al., 2005); (8) superior temporal sulcus, with rostroposterior and caudoposterior superior temporal sulcus (Fan et al., 2016); (9) posterior cingulate cortex, including dorsal, caudal and ventral area 23 and caudodorsal area 24 from Fan parcellation plus marginal branch of the cingulate sulcus from FreeSurfer parcellation; (10) inferior frontal gyrus, including area 44 with its dorsal, opercular, and ventral parts, and area 45 with its caudal part (Eickhoff et al., 2005; Fan et al., 2016); (11) parietal operculum, with areas OP1, OP2, OP3, and OP4 (Eickhoff et al., 2005); (12) posterior insula, including area Ig1 and Ig2 (granular insula; Eickhoff

et al., 2005), hypergranular insula (Fan et al., 2016), dorsal granular insula (Fan et al., 2016) and ventral dysgranular and granular insula (Fan et al., 2016); (13) middle insula, including area Id1 (dysgranular insula; Eickhoff et al., 2005) and dorsal dysgranular insula; (14) premotor cortex, including caudal dorsolateral and caudal ventrolateral area 6 (Fan et al., 2016); (15) superior parietal lobe, with intraparietal and postcentral area 7, area 7A, lateral area 5, as well as area 5Ci (Eickhoff et al., 2005); (16) precuneus, including dorsomedial parieto-occipital sulcus, regions 5 M (Eickhoff et al., 2005), 7 M (Eickhoff et al., 2005), medial area 7 (Fan et al., 2016), medial area 5 (Fan et al., 2016), and area 31 (Fan et al., 2016); (17) inferior parietal cortex, including rostroventral, rostrodorsal, and caudal area 39, rostroventral, rostrodorsal and caudal area 40 (Fan et al., 2016), area Pfm, area PF, area PFcm, area PFt, area PGp (Eickhoff et al., 2005); (18) visual-motion cortex, including regions V5/MT+ (Fan et al., 2016) and hOC5 (Eickhoff et al., 2005); (19) fusiform cortex including dorsolateral, ventrolateral, medioventral and lateroventral area 37 (Fan et al., 2016). For the calculation of the FDR corrected statistical threshold, we used an expanded connectivity matrix, which included these additional 19 regions. We also built a diagram of *autonomic–vestibular interactions*, by showing the connectivity of the Ve with autonomic regions.

3 | RESULTS

3.1 | Functional connectome of autonomic, pain, limbic, and sensory nuclei

The connectivity matrix, 2D circular connectome, nodal graph measures of all autonomic, pain, limbic and sensory brainstem nuclei are shown in Figure 1. Figure 1a shows the connectivity matrix ($-\log_{10}(p$ values)) of all (27) brainstem nuclei with 227 cortical and subcortical regions. FDR corrected threshold of $p < .0005$ was used for display purposes. These connectivity values were displayed as a 2D circular connectome in Figure 1b. We observed denser connectivity within the brainstem as compared to the connectivity of the brainstem with cortex/subcortex. In Figure 1c, we display results of nodal measures of graph analysis of each seed, such as degree centrality and normalized participant coefficient. VTA-PBP, LPB, MPB, Ve, PCRtA, SOC, sMRt, VSM, iMRt, ROb, and RPa showed above mean degree centrality, quantifying local centrality of these seeds, and indicating their direct neurobiological significance in the present network analysis. In our connectome, VTA-PBP, MiTg-PBG, LPB, MPB, Ve, PCRtA, SOC, sMRt, iMRt, RMg, ROb, and RPa seeds showed above average values of normalized participant coefficient, indicating their ability in keeping communication between their own module and the other modules. The laterality indices were below 26.5% for all seeds (SC = 14.4%, IC = 16.0%, VTA-PBP = 15.9%, MiTg-PBG = 7.1%, LPB =8.8%, MPB = 17.9%, Ve = 14.1%, PCRtA = 8.8%, SOC = 8.8%, sMRt =12.3%, VSM = 26.5%, iMRt = 12.3%), thus left and right nuclei displayed near mirrored connectivity. Individual left sided nuclei involved in autonomic, pain, limbic, and sensory network showed

specific connectivity to other brain regions (see individual 2D connectomes in Figures 2–9). For display purposes, in Figures 2–9 the mean tract density for each seed was also displayed as streamline density map (*p* < .05, uncorrected).

3.2 | 7 Tesla versus 3 Tesla results

The association between 7 Tesla and 3 Tesla mean connectivity indices in whole brain targets (*r* = .50, *p* < 1.4e−51), brainstem only targets (*r* = .37, *p* = 1.4e−51) and cortical/subcortical (other than brainstem) targets (*r* = .63, *p* < 1.4e−51) was moderate/high (Figure 10a). The percentage of common links between 7 Tesla and 3 Tesla data decreased with increasing the statistical significance threshold (Figure 10b); for a *p* = 0.05 FDR corrected, it was equal to 97.1, 74.5, and 66.7% for brainstem only targets, whole brain targets, and cortical/other subcortical targets, respectively. These results show good translatability of 7 Tesla results into a conventional dataset acquired at 3 Tesla. The translatability decreased for more conservative thresholds. For instance, for a *p* = .0005 FDR corrected, it was equal to 71.01, 31.33, and 17.71% for brainstem only targets, whole brain targets, and cortical/other subcortical targets, respectively.

3.3 | Circuit diagram generation

The resulting 2D connectome was used to build three circuit diagrams (Figure 11) along with their connection strengths, relating to (i) autonomic, pain, limbic, and sensory network, (ii) vestibular network, and (iii) autonomic–vestibular interaction network. Specifically, we generated a schematic diagram of these network circuits, using as nodes the brainstem nuclei and cortical regions involved in each function based on human and animal literature, and as links the connectivity values of our human connectome.

4 | DISCUSSION

This study provided a structural connectome of human brainstem nuclei involved in autonomic, pain, sensory, and reflexive emotional functions. Despite their involvement in critical functions, the study of these tiny brainstem nuclei in living humans is challenging due to the difficulty of visualizing them in conventional imaging due to limited resolution and contrast of conventional MRI. In this work, we used a high-spatial resolution brainstem nuclei atlas developed at 7 Tesla and diffusion-weighted data acquired at high-resolution (at 7 Tesla) and clinical resolution (at 3 Tesla for showing translatability) to provide individual structural connectomes of brainstem nuclei involved in autonomic, pain, sensory, and reflexive emotional functions. A summary of major connectivity findings of autonomic, pain, limbic, and sensory brainstem nuclei in line with literature is reported in Table 2. Here, we individually discuss the resulting structural connectivity of these nuclei in the context of animal and human literature. Then we

discuss graph-based network analysis results to unravel system-level topological properties of brainstem-brain connectivity in this network. Further, we also review the translational capability of our results to clinical setting (3 Tesla MRI) thereby providing evidence of greater applicability in healthy and disease population. Finally, we explore network circuits generated from a system neuroscience perspective and discuss specific links based on human and animal literature.

4.1 | Comparative analysis of our structural connectome with existing literature

The **superior colliculus (SC)** is involved in the orientation of the head and senses toward objects of interest. It displayed a link with the IC, in agreement with the literature finding that it receives afferents from the IC making up the auditory map of SC (Mellott, Beebe, & Schofield, 2018), as well as from the auditory nucleus SOC. In line with recent study in rodents underlying its involvement in defensive behavior, we also found SC connectivity to PBG (Deichler et al., 2020). Interestingly, SC also showed connectivity with the mRt and isRT that participate in horizontal saccades and head movements as shown in primate studies (Cohen & Büttner-Ennever, 1984; May, 2006; N. Wang, Warren, & May, 2010). In concordance with evidence of involvement in visuomotor activity, we found SC connectivity to the visual cortex, medial temporal cortex, frontal eye fields (compatible to G-frontal-sup, G-frontal-middle, S-frontal-sup, and S-frontal-middle in our connectomes; Huerta, Krubitzer, & Kaas, 1986; Stanton, Goldberg, & Bruce, 1988) and the supplementary eye fields (with a comparable location to S-precentral-sup-part and G- and S-paracentral in our connectomes; Huerta & Kaas, 1990; Shook, Schlag-Rey, & Schlag, 1990) parietal eye fields (S- intraparietal), thalamus (Harting & Updyke, 2006), striatum (caudate, putamen, and basal forebrain), sMRt (gigantocellular reticular nucleus; Quessy & Freedman, 2004), substantia nigra reticulata (SNr) compatible with SN1, PTg, LC, and PnO-PnC, which modulates horizontal saccadic eye movements (May, 2006).
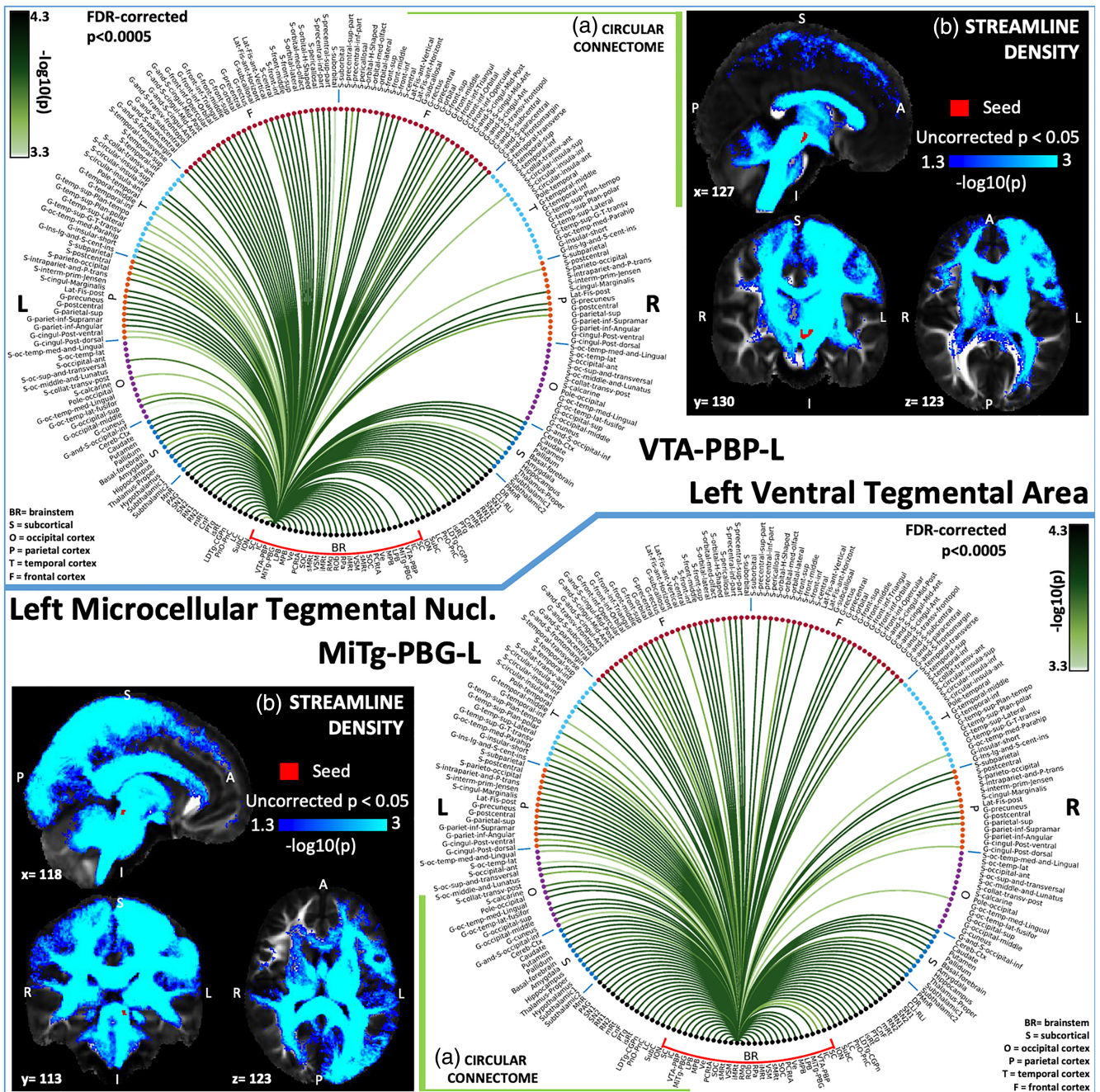
The **inferior colliculus (IC)** acts as an auditory relay transmitting parallel pathways from all auditory brainstem nuclei to ipsilateral thalamus and cerebral cortex. Neuroanatomical data shows that IC is also connected to deep layers of SC (containing maps for both visual and auditory fields; May, 2006). This was observed in our connectome where we found strong connectivity of IC with SC, SOC, primary auditory cortex (G-temp Sup Tranverse region), and primary visual cortex (S-calcarine). IC also showed strong connectivity with thalamus. The external IC is a multisensory region which receives retinal, somatosensory, spinal trigeminal and spinal dorsal column nuclear afferents, as well as inputs from the substantia nigra and the cerebral cortex (Coleman & Clerici, 1987). The observed strong connectivity of IC with substantia nigra and cerebral cortex is in line with these findings.

The **ventral tegmental area with parabrachial pigmented nucleus of the ventral tegmental area nuclei complex (VTA-PBP),** consisting of VTA, PBP, interpeduncular nucleus, caudal subnucleus (IPC), interpeduncular fossa (PIF), parapeduncular nucleus (PaP), paranigral
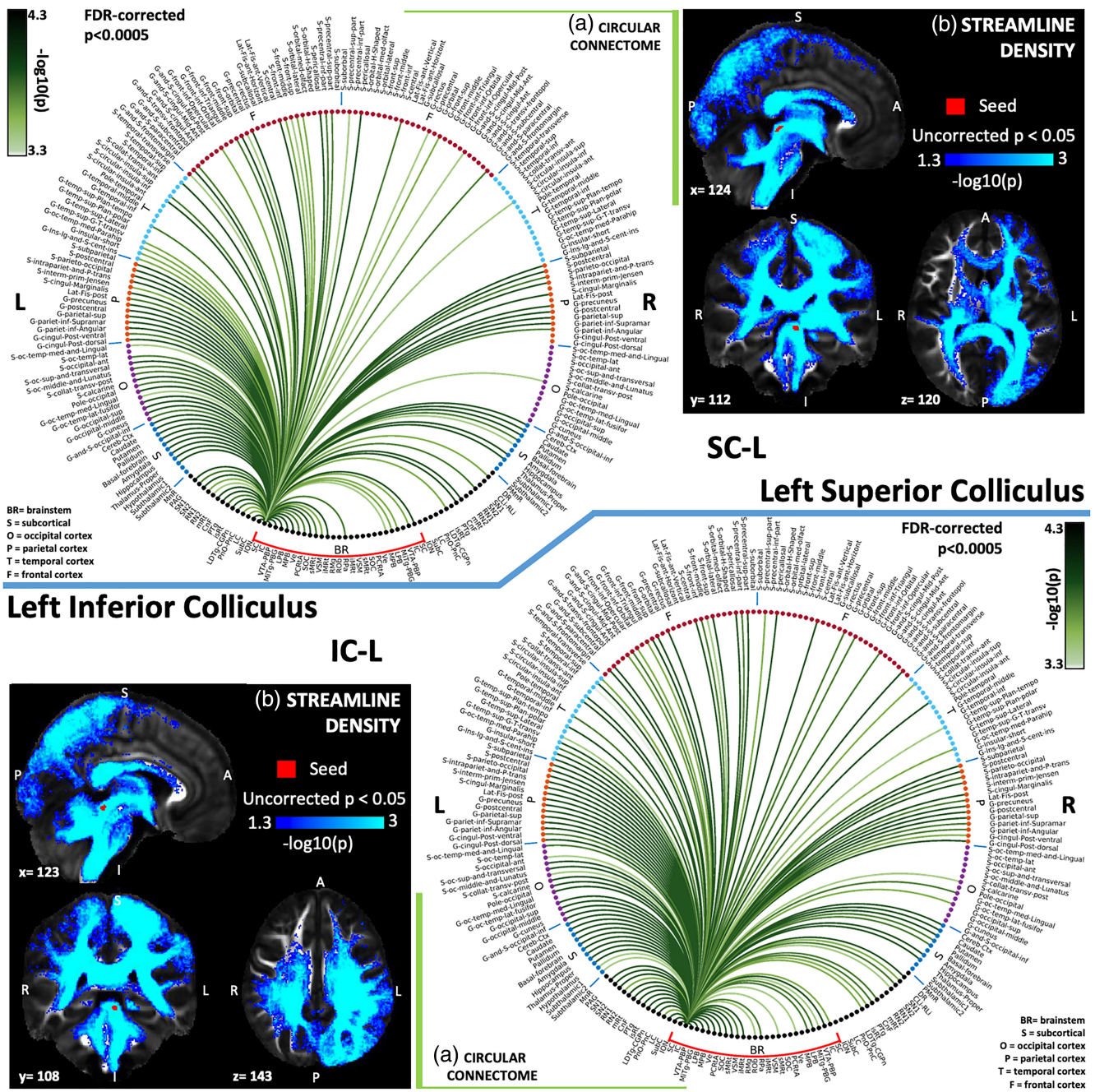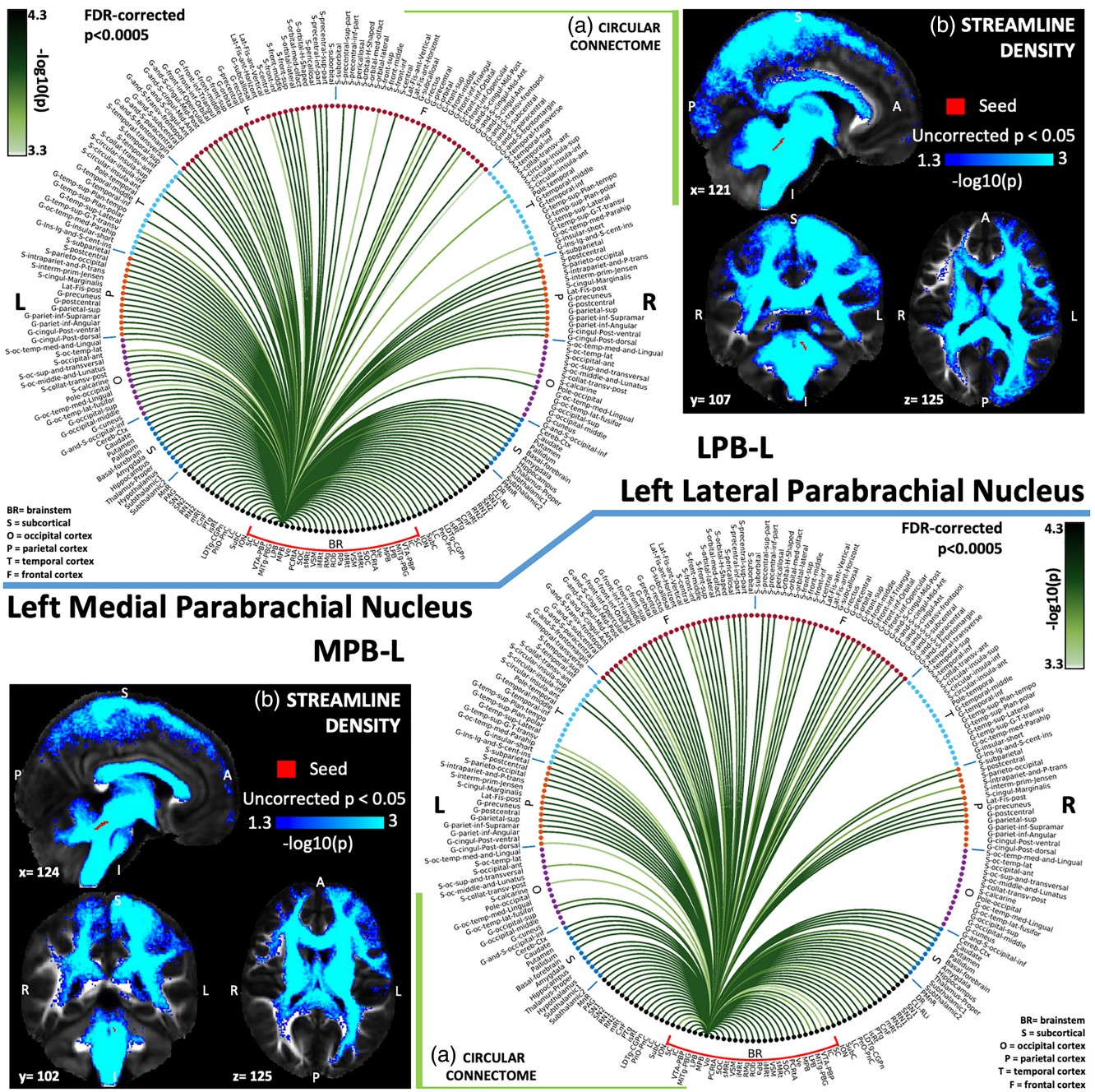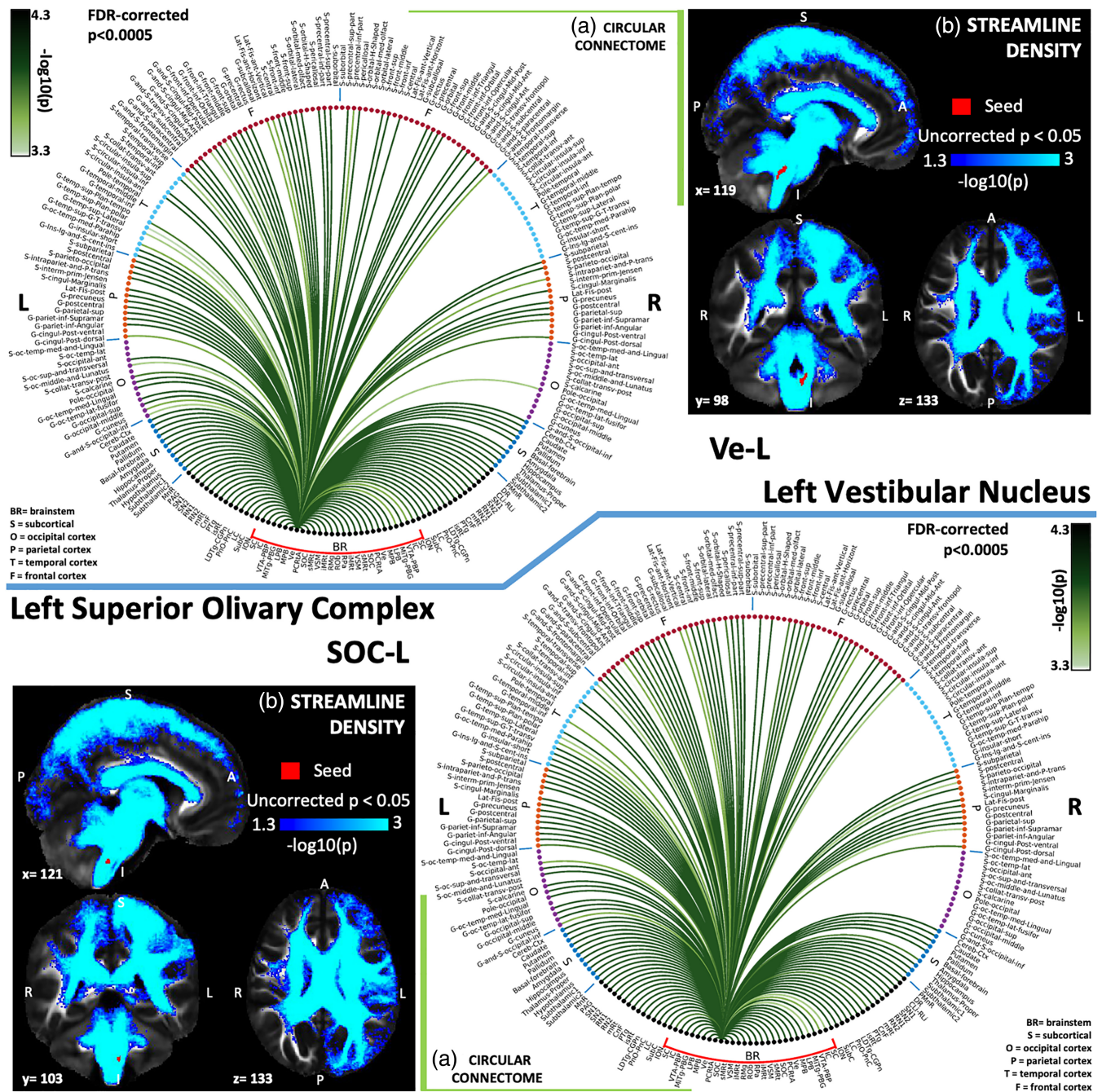
FIGURE 2 (a) Region-based 2D structural connectome and (b) voxel-based streamline density map of left superior colliculus—SC-L (top) and left inferior colliculus—IC-L (bottom). Specifically, in (a) we show the −log₁₀(p value) of the Wilcoxon test, thresholded, for display purposes, at p < .0005 false discovery rate (FDR) corrected for multiple comparisons. In (b) we show the −log₁₀(p value) of the Wilcoxon test thresholded, for display purposes, at p < .05; seeds are shown in red and streamlines are shown in blue-light blue. List of abbreviations of 15 brainstem nuclei used as seeds (marked with red brackets in Figure 1a,b): superior colliculus (SC), inferior colliculus (IC), ventral tegmental area-parabrachial pigmented nucleus (VTA-PBP), microcellular tegmental nucleus–parabigeminal nucleus (MiTg-PBG), lateral parabrachial nucleus (LPB), medial parabrachial nucleus (MPB), vestibular nuclei complex (Ve), parvicellular reticular nucleus-alpha part (PCRtA), superior olivary complex (SOC), superior medullary reticular formation (sMRt), viscerosensory motor nuclei complex (VSM), inferior medullary reticular formation (iMRt), raphe magnus (RMg), raphe obscurus (ROb) and raphe pallidus (RPa). List of abbreviations of 18 additional brainstem nuclei used as targets: median raphe nucleus (MnR), periaqueductal gray (PAG), substantia nigra-subregion1 (SN1), substantia nigra-subregion2 (SN2), red nucleus-subregion1 (RN1), red nucleus-subregion2 (RN2), mesencephalic reticular formation (mRt), cuneiform nucleus (CnF), pedunculotegmental nucleus (PTg), isthmic reticular formation (isRt), laterodorsal tegmental nucleus–central gray of the rhombencephalon (LDTg-CGPn), pontine reticular nucleus, oral part–pontine reticular nucleus, caudal part (PnO-PnC), locus coeruleus (LC), subcoeruleus nucleus (SubC), inferior olivary nucleus (ION), caudal–rostral linear raphe (CLi-RLi), dorsal raphe (DR), and paramedian raphe nucleus (PMnR).
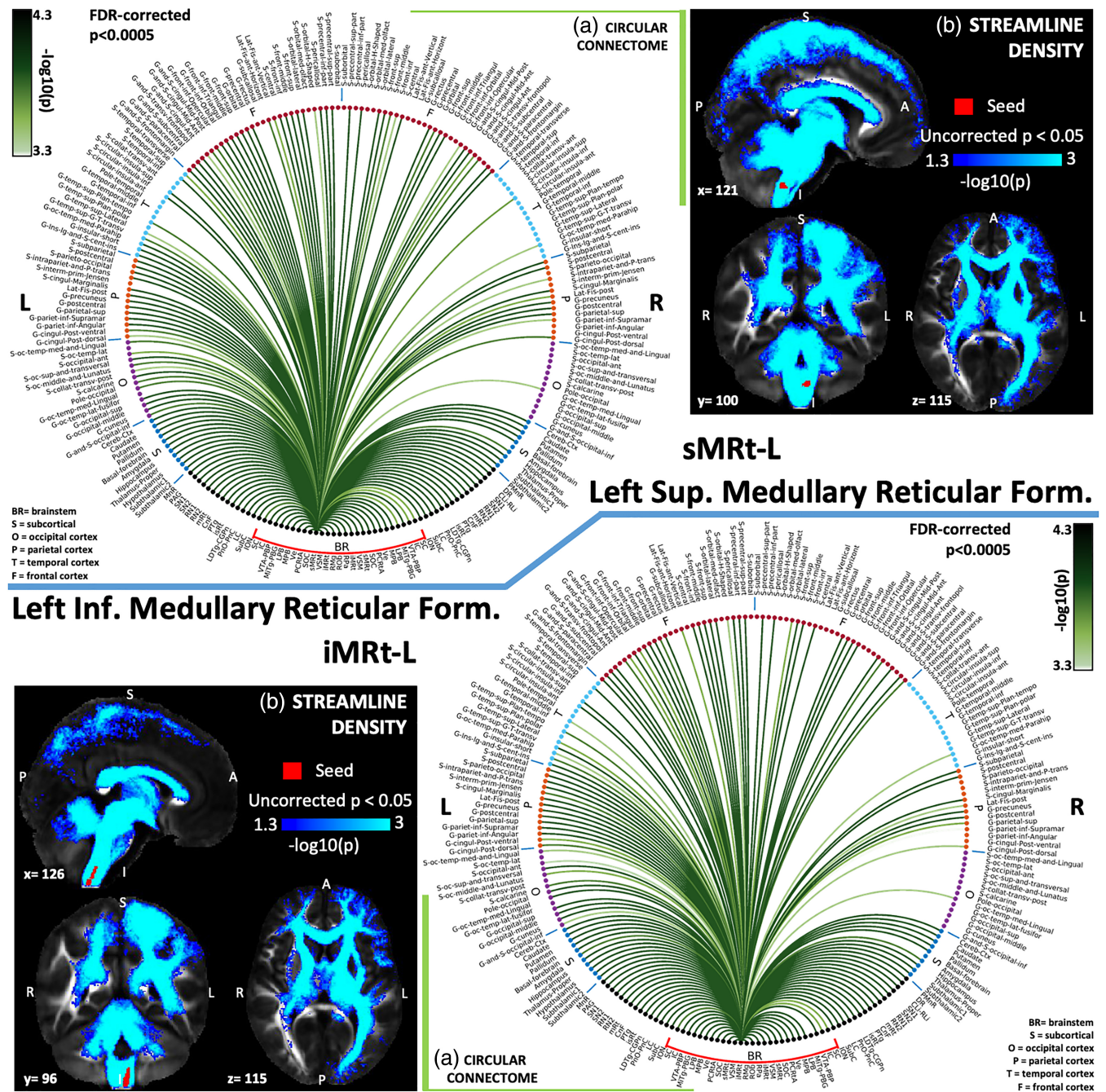
FIGURE 3 (a) Region-based 2D structural connectome and (b) voxel-based streamline density map of left ventral tegmental area—VTA-PBP-L (top) and left microcellular tegmental nucleus–parabigeminal nucleus—MiTg-PBG-L (bottom). Specifically, in (a) we show the −log$_{10}$(p value) of the Wilcoxon test, thresholded, for display purposes, at $p < .0005$ false discovery rate (FDR) corrected for multiple comparisons. In (b) we show the −log$_{10}$(p value) of the Wilcoxon test thresholded, for display purposes, at $p < .05$; seeds are shown in red and streamlines are shown in blue-light blue. List of abbreviations of 15 brainstem nuclei used as seeds (marked with red brackets in Figure 1a,b): superior colliculus (SC), inferior colliculus (IC), ventral tegmental area-parabrachial pigmented nucleus (VTA-PBP), microcellular tegmental nucleus–parabigeminal nucleus (MiTg-PBG), lateral parabrachial nucleus (LPB), medial parabrachial nucleus (MPB), vestibular nuclei complex (Ve), parvicellular reticular nucleus-alpha part (PCRtA), superior olivary complex (SOC), superior medullary reticular formation (sMRt), viscerosensory motor nuclei complex (VSM), inferior medullary reticular formation (iMRt), raphe magnus (RMg), raphe obscurus (ROb) and raphe pallidus (RPa). List of abbreviations of 18 additional brainstem nuclei used as targets: median raphe nucleus (MnR), periaqueductal gray (PAG), substantia nigra-subregion1 (SN1), substantia nigra-subregion2 (SN2), red nucleus-subregion1 (RN1), red nucleus-subregion2 (RN2), mesencephalic reticular formation (mRt), cuneiform nucleus (CnF), pedunculotegmental nucleus (PTg), isthmic reticular formation (isRt), laterodorsal tegmental nucleus–central gray of the rhombencephalon (LDTg-CGPn), pontine reticular nucleus, oral part–pontine reticular nucleus, caudal part (PnO-PnC), locus coeruleus (LC), subcoeruleus nucleus (SubC), inferior olivary nucleus (ION), caudal–rostral linear raphe (CLi-RLi), dorsal raphe (DR), and paramedian raphe nucleus (PMnR)
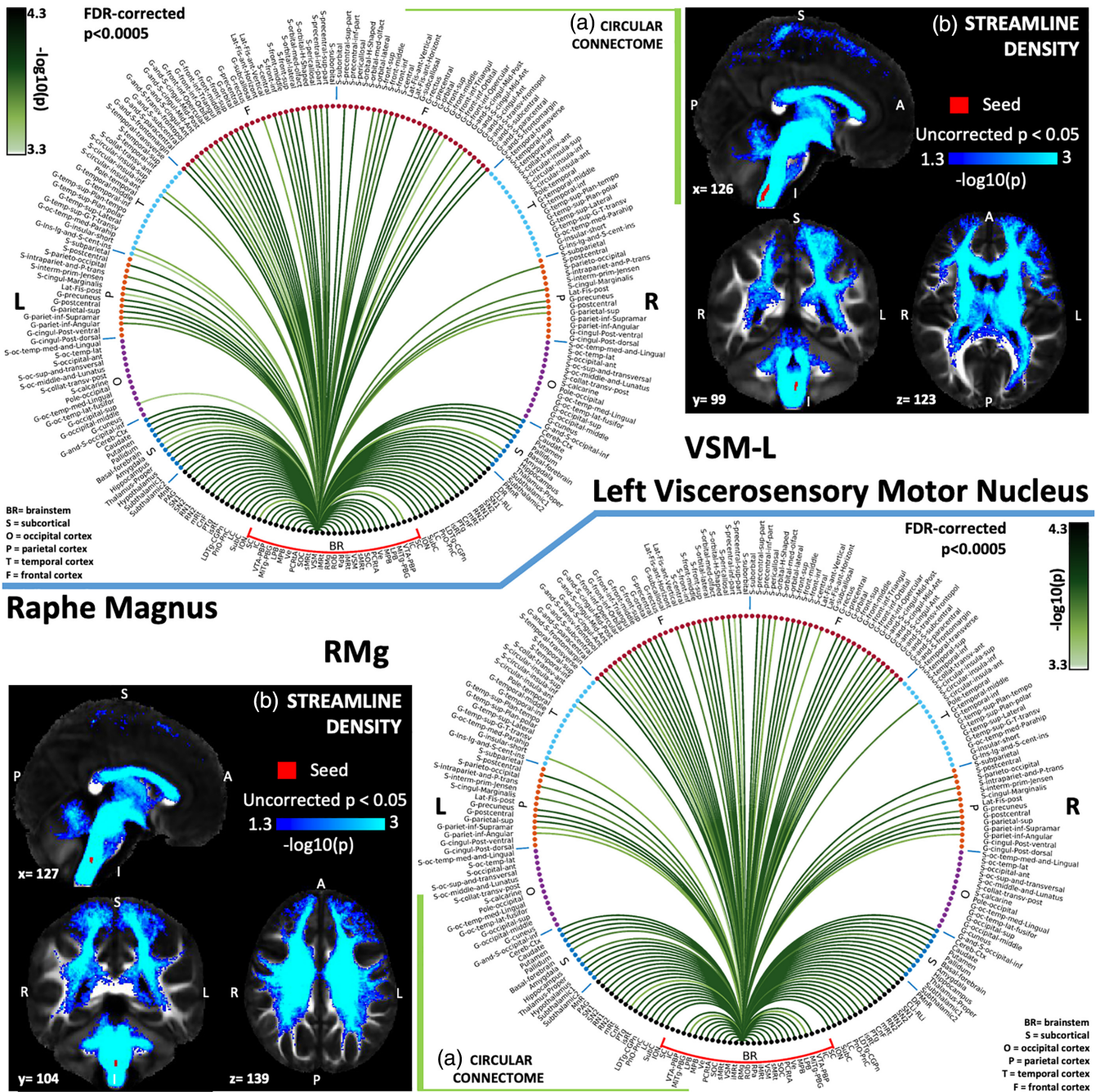
FIGURE 4 (a) Region-based 2D structural connectome and (b) voxel-based streamline density map of left lateral parabrachial nucleus—LPB-L (top) and left medial parabrachial nucleus—MPB-L (bottom). Specifically, in (a) we show the $-\log_{10}(p$ value) of the Wilcoxon test, thresholded, for display purposes, at $p < .0005$ false discovery rate (FDR) corrected for multiple comparisons. In (b) we show the $-\log_{10}(p$ value) of the Wilcoxon test thresholded, for display purposes, at $p < .05$; seeds are shown in red and streamlines are shown in blue-light blue. List of abbreviations of 15 brainstem nuclei used as seeds (marked with red brackets in Figure 1a,b): superior colliculus (SC), inferior colliculus (IC), ventral tegmental area-parabrachial pigmented nucleus (VTA-PBP), microcellular tegmental nucleus–parabigeminal nucleus (MiTg-PBG), lateral parabrachial nucleus (LPB), medial parabrachial nucleus (MPB), vestibular nuclei complex (Ve), parvicellular reticular nucleus-alpha part (PCRtA), superior olivary complex (SOC), superior medullary reticular formation (sMRt), viscerosensory motor nuclei complex (VSM), inferior medullary reticular formation (iMRt), raphe magnus (RMg), raphe obscurus (ROb) and raphe pallidus (RPa). List of abbreviations of 18 additional brainstem nuclei used as targets: median raphe nucleus (MnR), periaqueductal gray (PAG), substantia nigra-subregion1 (SN1), substantia nigra-subregion2 (SN2), red nucleus-subregion1 (RN1), red nucleus-subregion2 (RN2), mesencephalic reticular formation (mRt), cuneiform nucleus (CnF), pedunculotegmental nucleus (PTg), isthmic reticular formation (isRt), laterodorsal tegmental nucleus–central gray of the rhombencephalon (LDTg-CGPn), pontine reticular nucleus, oral part–pontine reticular nucleus, caudal part (PnO-PnC), locus coeruleus (LC), subcoeruleus nucleus (SubC), inferior olivary nucleus (ION), caudal–rostral linear raphe (CLi-RLi), dorsal raphe (DR), and paramedian raphe nucleus (PMnR)
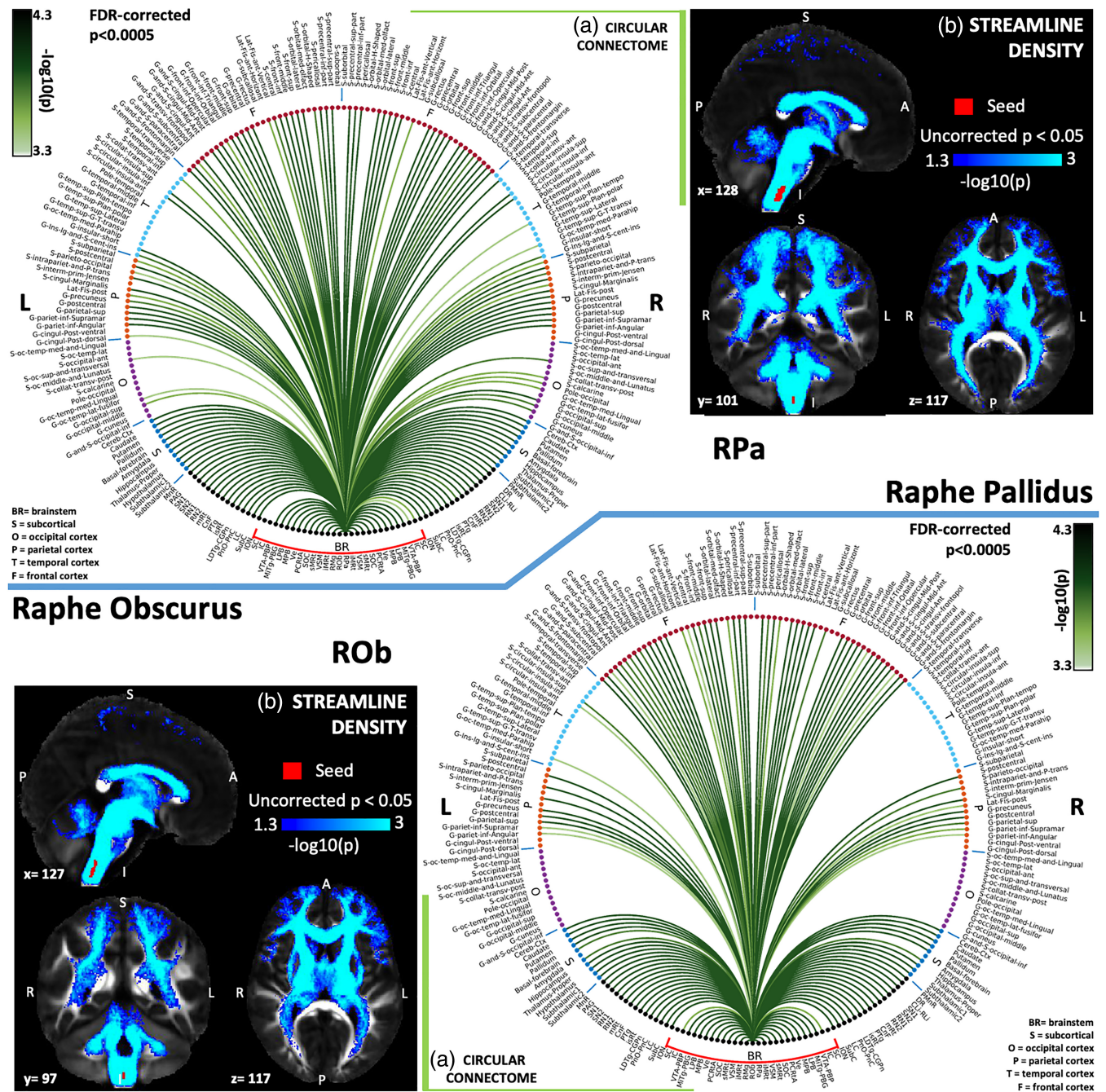
FIGURE 5 (A) Region-based 2D structural connectome and (b) voxel-based streamline density map of left vestibular nucleus—Ve-L (top) and left superior olivary complex—SOC-L (bottom). Specifically, in (a) we show the −log₁₀(p value) of the Wilcoxon test, thresholded, for display purposes, at p < .0005 false discovery rate (FDR) corrected for multiple comparisons. In (b) we show the −log₁₀(p value) of the Wilcoxon test thresholded, for display purposes, at p < .05; seeds are shown in red and streamlines are shown in blue-light blue. List of abbreviations of 15 brainstem nuclei used as seeds (marked with red brackets in Figure 1a,b): superior colliculus (SC), inferior colliculus (IC), ventral tegmental area-parabrachial pigmented nucleus (VTA-PBP), microcellular tegmental nucleus–parabigeminal nucleus (MiTg-PBG), lateral parabrachial nucleus (LPB), medial parabrachial nucleus (MPB), vestibular nuclei complex (Ve), parvicellular reticular nucleus-alpha part (PCRtA), superior olivary complex (SOC), superior medullary reticular formation (sMRt), viscerosensory motor nuclei complex (VSM), inferior medullary reticular formation (iMRt), raphe magnus (RMg), raphe obscurus (ROb), and raphe pallidus (RPa). List of abbreviations of 18 additional brainstem nuclei used as targets: median raphe nucleus (MnR), periaqueductal gray (PAG), substantia nigra-subregion1 (SN1), substantia nigra-subregion2 (SN2), red nucleus-subregion1 (RN1), red nucleus-subregion2 (RN2), mesencephalic reticular formation (mRt), cuneiform nucleus (CnF), pedunculotegmental nucleus (PTg), isthmic reticular formation (isRt), laterodorsal tegmental nucleus–central gray of the rhombencephalon (LDTg-CGPn), pontine reticular nucleus, oral part–pontine reticular nucleus, caudal part (PnO-PnC), locus coeruleus (LC), subcoeruleus nucleus (SubC), inferior olivary nucleus (ION), caudal–rostral linear raphe (CLi-RLi), dorsal raphe (DR), and paramedian raphe nucleus (PMnR)
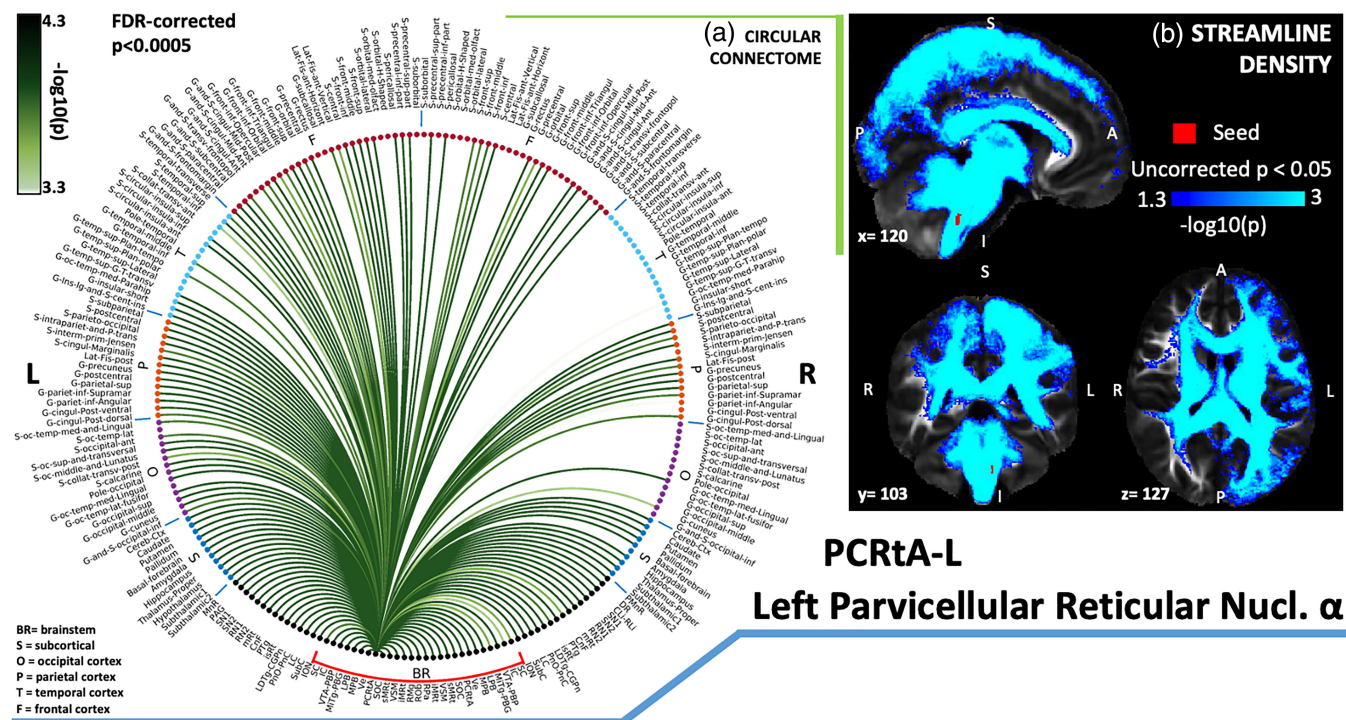
FIGURE 6 (a) Region-based 2D structural connectome and (b) voxel-based streamline density map of left superior medullary reticular formation—sMRt-L (top) and left inferior medullary reticular formation—iMRt-L (bottom). Specifically, in (a) we show the −log$_{10}$(p value) of the Wilcoxon test, thresholded, for display purposes, at $p < .0005$ false discovery rate (FDR) corrected for multiple comparisons. In (b) we show the −log$_{10}$(p value) of the Wilcoxon test thresholded, for display purposes, at $p < .05$; seeds are shown in red and streamlines are shown in blue-light blue. List of abbreviations of 15 brainstem nuclei used as seeds (marked with red brackets in Figure 1a,b): superior colliculus (SC), inferior colliculus (IC), ventral tegmental area-parabrachial pigmented nucleus (VTA-PBP), microcellular tegmental nucleus–parabigeminal nucleus (MiTg-PBG), lateral parabrachial nucleus (LPB), medial parabrachial nucleus (MPB), vestibular nuclei complex (Ve), parvicellular reticular nucleus-alpha part (PCRtA), superior olivary complex (SOC), superior medullary reticular formation (sMRt), viscerosensory motor nuclei complex (VSM), inferior medullary reticular formation (iMRt), raphe magnus (RMg), raphe obscurus (ROb), and raphe pallidus (RPa). List of abbreviations of 18 additional brainstem nuclei used as targets: median raphe nucleus (MnR), periaqueductal gray (PAG), substantia nigra-subregion1 (SN1), substantia nigra-subregion2 (SN2), red nucleus-subregion1 (RN1), red nucleus-subregion2 (RN2), mesencephalic reticular formation (mRt), cuneiform nucleus (CnF), pedunculotegmental nucleus (PTg), isthmic reticular formation (isRt), laterodorsal tegmental nucleus–central gray of the rhombencephalon (LDTg-CGPn), pontine reticular nucleus, oral part–pontine reticular nucleus, caudal part (PnO-PnC), locus coeruleus (LC), subcoeruleus nucleus (SubC), inferior olivary nucleus (ION), caudal–rostral linear raphe (CLi-RLi), dorsal raphe (DR), and paramedian raphe nucleus (PMnR)

FIGURE 7 (a) Region-based 2D structural connectome and (b) voxel-based streamline density map of left viscerosensory motor nucleus—VSM-L (top) and raphe magnus—RMg (bottom). Specifically, in (a) we show the $-\log_{10}(p$ value) of the Wilcoxon test, thresholded, for display purposes, at $p < .0005$ false discovery rate (FDR) corrected for multiple comparisons. In (b) we show the $-\log_{10}(p$ value) of the Wilcoxon test thresholded, for display purposes, at $p < .05$; seeds are shown in red and streamlines are shown in blue-light blue. List of abbreviations of 15 brainstem nuclei used as seeds (marked with red brackets in Figure 1a,b): superior colliculus (SC), inferior colliculus (IC), ventral tegmental area-parabrachial pigmented nucleus (VTA-PBP), microcellular tegmental nucleus–parabigeminal nucleus (MiTg-PBG), lateral parabrachial nucleus (LPB), medial parabrachial nucleus (MPB), vestibular nuclei complex (Ve), parvicellular reticular nucleus-alpha part (PCRtA), superior olivary complex (SOC), superior medullary reticular formation (sMRt), viscerosensory motor nuclei complex (VSM), inferior medullary reticular formation (iMRt), raphe magnus (RMg), raphe obscurus (ROb), and raphe pallidus (RPa). List of abbreviations of 18 additional brainstem nuclei used as targets: median raphe nucleus (MnR), periaqueductal gray (PAG), substantia nigra-subregion1 (SN1), substantia nigra-subregion2 (SN2), red nucleus-subregion1 (RN1), red nucleus-subregion2 (RN2), mesencephalic reticular formation (mRt), cuneiform nucleus (CnF), pedunculotegmental nucleus (PTg), isthmic reticular formation (isRt), laterodorsal tegmental nucleus–central gray of the rhombencephalon (LDTg-CGPn), pontine reticular nucleus, oral part–pontine reticular nucleus, caudal part (PnO-PnC), locus coeruleus (LC), subcoeruleus nucleus (SubC), inferior olivary nucleus (ION), caudal–rostral linear raphe (CLi-RLi), dorsal raphe (DR), and paramedian raphe nucleus (PMnR)

FIGURE 8 (a) Region-based 2D structural connectome and (b) voxel-based streamline density map of raphe pallidus—RPa (top) and raphe obscurus—ROb (bottom). Specifically, in (a) we show the $-\log_{10}(p$ value) of the Wilcoxon test, thresholded, for display purposes, at $p < .0005$ false discovery rate (FDR) corrected for multiple comparisons. In (b) we show the $-\log_{10}(p$ value) of the Wilcoxon test thresholded, for display purposes, at $p < .05$; seeds are shown in red and streamlines are shown in blue-light blue. List of abbreviations of 15 brainstem nuclei used as seeds (marked with red brackets in Figure 1a,b): superior colliculus (SC), inferior colliculus (IC), ventral tegmental area-parabrachial pigmented nucleus (VTA-PBP), microcellular tegmental nucleus–parabigeminal nucleus (MiTg-PBG), lateral parabrachial nucleus (LPB), medial parabrachial nucleus (MPB), vestibular nuclei complex (Ve), parvicellular reticular nucleus-alpha part (PCRtA), superior olivary complex (SOC), superior medullary reticular formation (sMRt), viscerosensory motor nuclei complex (VSM), inferior medullary reticular formation (iMRt), raphe magnus (RMg), raphe obscurus (ROb), and raphe pallidus (RPa). List of abbreviations of 18 additional brainstem nuclei used as targets: median raphe nucleus (MnR), periaqueductal gray (PAG), substantia nigra-subregion1 (SN1), substantia nigra-subregion2 (SN2), red nucleus-subregion1 (RN1), red nucleus-subregion2 (RN2), mesencephalic reticular formation (mRt), cuneiform nucleus (CnF), pedunculotegmental nucleus (PTg), isthmic reticular formation (isRt), laterodorsal tegmental nucleus–central gray of the rhombencephalon (LDTg-CGPn), pontine reticular nucleus, oral part–pontine reticular nucleus, caudal part (PnO-PnC), locus coeruleus (LC), subcoeruleus nucleus (SubC), inferior olivary nucleus (ION), caudal–rostral linear raphe (CLi-RLi), dorsal raphe (DR), and paramedian raphe nucleus (PMnR)

FIGURE 9 (a) Region-based 2D structural connectome and (b) voxel-based streamline density map of left parvicellular reticular nucleus-alpha part—PCRtA-L. Specifically, in (a) we show the $-\log_{10}(p$ value) of the Wilcoxon test, thresholded, for display purposes, at $p < .0005$ false discovery rate (FDR) corrected for multiple comparisons. In (b) we show the $-\log_{10}(p$ value) of the Wilcoxon test thresholded, for display purposes, at $p < .05$; seeds are shown in red and streamlines are shown in blue-light blue. List of abbreviations of 15 brainstem nuclei used as seeds (marked with red brackets in Figure 1a,b): superior colliculus (SC), inferior colliculus (IC), ventral tegmental area-parabrachial pigmented nucleus (VTA-PBP), microcellular tegmental nucleus–parabigeminal nucleus (MiTg-PBG), lateral parabrachial nucleus (LPB), medial parabrachial nucleus (MPB), vestibular nuclei complex (Ve), parvicellular reticular nucleus-alpha part (PCRtA), superior olivary complex (SOC), superior medullary reticular formation (sMRt), viscerosensory motor nuclei complex (VSM), inferior medullary reticular formation (iMRt), raphe magnus (RMg), raphe obscurus (ROb), and raphe pallidus (RPa). List of abbreviations of 18 additional brainstem nuclei used as targets: median raphe nucleus (MnR), periaqueductal gray (PAG), substantia nigra-subregion1 (SN1), substantia nigra-subregion2 (SN2), red nucleus-subregion1 (RN1), red nucleus-subregion2 (RN2), mesencephalic reticular formation (mRt), cuneiform nucleus (CnF), pedunculotegmental nucleus (PTg), isthmic reticular formation (isRt), laterodorsal tegmental nucleus–central gray of the rhombencephalon (LDTg-CGPn), pontine reticular nucleus, oral part–pontine reticular nucleus, caudal part (PnO-PnC), locus coeruleus (LC), subcoeruleus nucleus (SubC), inferior olivary nucleus (ION), caudal–rostral linear raphe (CLi-RLi), dorsal raphe (DR), and paramedian raphe nucleus (PMnR)

nucleus of ventral tegmental area (PN), interpeduncular nucleus, dorsomedial subnucleus (IPDM), and interfascicular nucleus (IF; Singh et al., 2021) has been implicated in reward system, motivation, cognition, drug addiction, avoidance, fear conditioning, and arousal (Eban-Rothschild, Rothschild, Giardino, Jones, & de Lecea, 2016; Edlow et al., 2012; Tang et al., 2020; Wise, 2004; Wu, Boyle, & Palmiter, 2009). PN and IFN have been linked to limbic and thalamic pathways to forebrain, whereas PBP has been linked to striatal and cortical pathways to the forebrain. In our current work, we found VTA-PBP connectivity with the prefrontal cortex, in line with results from Wager and Cox (Wager & Cox, 2009), with PTg and LDTg, in line with data from Mena-Segovia (Mena-Segovia, 2016). In addition we found VTA-PBP connectivity with thalamus (subthalamic nucleus, bed nucleus of the stria terminalis), SC, PAG, DR, and hypothalamus (lateral hypothalamic and preoptic areas; Hosp et al., 2019; Morales & Margolis, 2017; Morikawa & Paladini, 2011), which were shown to be its glutamatergic/cholinergic afferents. VTA-PBP also showed

connectivity to basal forebrain and ventral pallidum, which are GABAergic afferents of VTA (Morales & Margolis, 2017). VTA has also efferent projections to these regions along with amygdala (Chuhma, Mingote, Moore, & Rayport, 2014; Tang et al., 2020), entorhinal cortex (G_occipit-temp_med-Parahippocampal_part), cingulate gyrus, hippocampus, and olfactory bulb. Links to these all of these regions, except for the olfactory bulb, which we do not include in this study, were also visible in the VTA-PBP structural connectome. In line with our results, PBP has been shown to connect via dopaminergic neurons to the nucleus accumbens (basal forebrain in our connectome) and via glutamatergic projections to the prefrontal cortex (Yamaguchi, Wang, Li, Ng, & Morales, 2011). PBP also was found to connect to the VTA (Halliday, Reyes, & Double, 2012), SNc (compatible with the link to SN2 in our connectome) and retrorubral fields (Halliday et al., 2012).

The **microcellular tegmental nucleus with parabigeminal nucleus (MiTg-PBG)** is involved in rapid response to threat before the signals are analyzed consciously (Usunoff et al., 2007). Interestingly, it
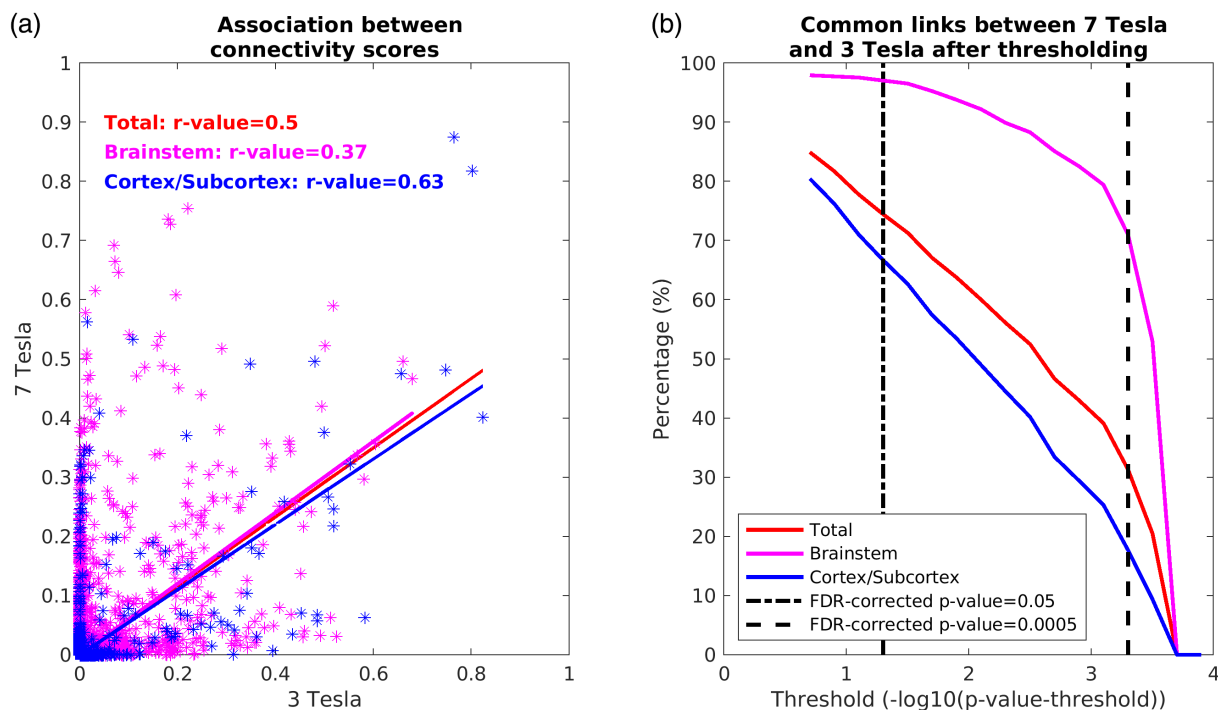
FIGURE 10 Translatability of high-resolution 7 Tesla structural connectome results to clinical resolution dataset acquired at 3 Tesla. (a) Association values between connectivity scores (averaged across participants and unthresholded) obtained at 3 Tesla and 7 Tesla for all the targets (red), brainstem only targets (magenta), and cortical/subcortical (other than brainstem, blue) targets. (b) Percentage of links in common between 7 Tesla versus 3 Tesla results found in the whole brain, brainstem and cortex/subcortex. A good association of values and a high number of common links across scanners at $p < .05$ FDR corrected suggests translatability of the brainstem nuclei connectome in clinical scanners at this statistical threshold, especially in the brainstem. Note, the decline in the number of common links across scanners with increasing the statistical threshold, especially for non-brainstem regions

showed connectivity with regions involved in this process such as amygdala (Usunoff et al., 2007). MiTg-PBG displayed a link with the SC, in line with findings of dense reciprocal interconnections of PBG with the superficial layers of the SC (Deichler et al., 2020). Our connectome of MiTg-PBG also is consistent with evidence of connectivity with prepositus nucleus (PrP; VSM in our connectome), the ventral nucleus of the lateral geniculate body (part of Thalamus-Proper in our connectome), LC, CnF, PAG and the dorsomedial hypothalamic area (Baleydier & Magnin, 1979), and projections to the thalamic magnocellular and parvocellular layers of the lateral geniculate nucleus (Bickford et al., 2000; Harting, van Lieshout, & Feig, 1991; part of Thalamus-Proper in our connectome).

The **parabrachial nuclei (MPB, LPB)** are relay regions of viscerosensory information such as taste, pain, respiration and cardiovascular function received from medullary regions, which communicate with upper central autonomic forebrain structures (J. Olszewski & Baxter, 1954). In line with this evidence, our human connectome showed parabrachial nuclei connected to thalamus, hypothalamus, basal forebrain, and amygdala (Fulwiler & Saper, 1984; Moga, Saper, & Gray, 1990). It also showed connectivity to RMg, in keeping with a possible role in nociception (G. Holstege, 1988), and with the pontomedullary reticular formation (sMRt, iMRt) for cardiovascular and respiratory control (Saper & Loewy, 1980). It also showed connectivity to vestibular nuclei as expected from previous

work (Balaban, 2004). Previous studies suggested that MPB and LPB has similar connectivity but with some differences. MPB receives afferents (gustatory signals) from the rostral solitary nucleus (within VSM in our connectome) while LPB receives visceral signals from the caudal solitary nucleus (Naidich et al., 2009). They both project to thalamus but MPB also projects directly to four regions of the cerebral cortex: the granular insula cortex (primary taste cortex), the deep layers of the frontal cortex, the septa-olfactory area (S_orbital_medial-olfactory) and the infralimbic cortex (G-rectus, G-subcallosal; Pritchard, 2012; Saper & Loewy, 1980). Based on our current nuclei delineations and targets, exploring these differences are beyond the scope of the current work.

The **vestibular nuclei complex (Ve)** consisted of the lateral, medial, spinal, and superior vestibular nuclei, nucleus of vestibular efferents, magnocellular and parvicellular part of medial vestibular nucleus, and paravestibular nucleus (Singh et al., 2019). It showed connectivity with different functional domains relating to eye/head movement (cerebellum, ION, sMRt, and PCRtA; Tellegen et al., 2001), balance (thalamus, insula, parietal cortex), sleep–wake state (LC, DR, and LDTg-CGPn, gigantocellular reticular nucleus, lateral paragigantocellular nucleus-sMRt, PAG, SubC, PCRtA, paraMnR; Kompotis et al., 2019), and emotional regulation (LC, DR, amygdala, insula; Brandt & Dieterich, 2019; Shi et al., 2021). As visible in the vestibular circuit diagram (Figure 11b), Ve was connected to the ION, which acts
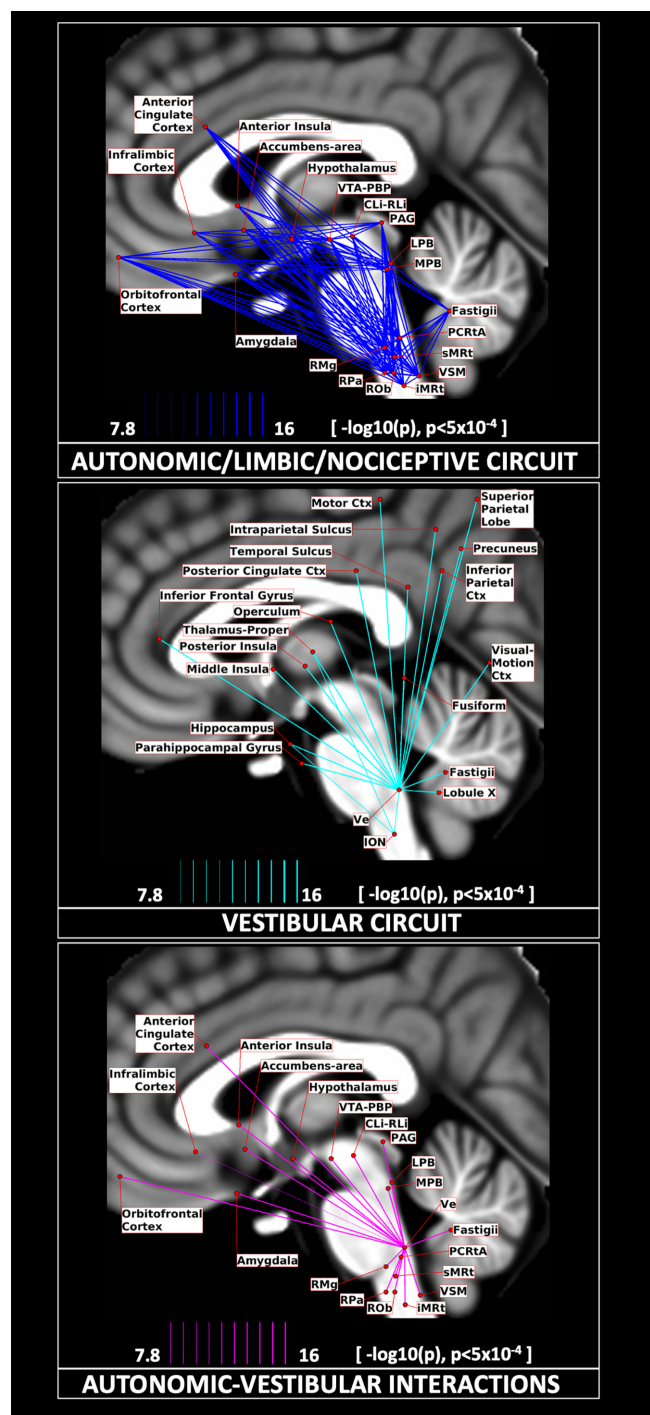
FIGURE 11 Circuit diagrams. We display the connectivity of two major networks involved in (a) autonomic/limbic/nociceptive function (top), vestibular function (middle), and their interaction (bottom). Their connections are displayed as solid lines with varying line thickness, proportional to its $-\log_{10}(p\ value)$, thresholded at $p < .005$, FDR corrected. The seeds and targets are represented as red circular nodes, with their centroid projected on the sagittal slice (coordinate $x = -2$ mm) of the T_1-weighted MNI template, with small adjustments in their positions to avoid node/link crowding

as a relay between Ve and the cerebellum (G. Olszewski & Baxter, 2014), where lobule X and fastigial nuclei are part of the vestibular network. We also found Ve connectivity extending to several

cortical and subcortical regions (Indovina et al., 2020) with particularly high connectivity values with the thalamus, insular cortex, cingulate cortex, and cerebellum, as also visible from the Ve circular connectome (Figure 5a). In nodal graph measure analysis, Ve displayed high degree centrality and normalized participant coefficient indicating high interconnectivity with neighboring regions and with distant cortical regions in different modules. We also investigated vestibular interactions with autonomic/limbic circuit, since autonomic/limbic-vestibular interactions have been studied as underlying pathophysiologic processes relating to chronic vestibular disorders (Brandt, 1996; Bronstein, 2004; Indovina et al., 2015; Jacob, Redfern, & Furman, 2009; Staab, 2012; Staab et al., 2017; Staab, Rohe, Eggers, & Shepard, 2014).

The **superior olivary complex (SOC)** is the first site of convergence of the cochlear input from the two ears and aids in detecting sounds in the horizontal plane (Webster, 1992). Mapping of interaural time differences is projected onto ipsilateral IC via the lateral lemniscus and relayed to the dorsal nucleus of the lateral lemniscus, which in turn sends GABAergic inhibitory projections to the contralateral IC and itself, as well as to the ipsilateral IC (Nieuwenhuys et al., 2008). In line with this evidence, we found strong connectivity of SOC to bilateral IC (Riemann & Reuss, 1998). SOC also displayed a link to thalamus as expected as part of the ascending auditory system. It also showed connectivity to primary auditory cortex (G-temp Sup Tranverse region; Coomes & Schofield, 2004).

The **superior medullary reticular formation (sMRt)** includes the compact part and the superior portion of the semicompact part of the nucleus ambiguus, the gigantocellular reticular nucleus, the parvicellular reticular nucleus, the intermediate reticular nucleus, the dorsal paragigantocellular nucleus, and the facial motor nucleus (García-Gomar, Videnovic, et al., 2021; Paxinos et al., 2012). The gigantocellular reticular nucleus (Gi) is reported to be involved in motor function (head, jaw, face, and tongue activity; Cowie & Robinson, 1994) and pain control via spinal cord and RMg (Westlund & Willis, 2012). As expected, it showed connectivity with VSM including hypoglossal nucleus in line with its involvement in medial somatic motor system (Blessing & Benarroch, 2012; Horn, 2006). Gi also showed connectivity with SC, Ve (head control), iMRt including ambiguus nucleus (Cowie & Robinson, 1994; Shinoda, Sugiuchi, Izawa, & Hata, 2006) and PAG (regulation of reflexive emotions) in line with previous studies (Gerrits et al., 2004; G. Holstege, 1991).

The **inferior medullary reticular formation (iMRt)** contains loose part and the inferior portion of the semicompact part of the ambiguus nucleus, as well as the retroambiguus nucleus, the ventral and dorsal medullary reticular nucleus, the intermediate reticular nucleus, noradrenaline cells A1 and adrenaline cells C1. The intermediate reticular nucleus is involved in postinspiratory activity, swallowing, and respiratory-sympathetic coupling. It was found to receive cholinergic inputs from hypoglossal nucleus in the rat (Volgin, Rukhadze, & Kubin, 2008), and was connected to VSM (including hypoglossal nucleus) in our human connectome. The dorsal medullary reticular nucleus is regarded as a supraspinal pain modulating area. In our results, we observed structural connectivity with ION, VSM, LC, LPB, MPB, PAG, SN1, SN2, and reticular nuclei as expected from studies in

TABLE 2 Summary of major connectivity findings of autonomic, pain, limbic, and sensory brainstem nuclei in line with literature

Brainstem nuclei	Connectivity
Superior colliculus (SC)	Auditory function: IC, SOC (May, 2006) Defensive behavior and orientation: PBG, SN1 (SNr), PTg, LC Horizontal saccades and head movements: mRt, isRt Visuomotor activity: Visual cortex, medial temporal cortex, frontal eye fields (compatible with G-frontal-sup, G-frontal-middle, S-frontal-sup and S-frontal-middle, supplementary eye fields (S-precentral-sup-part and G- and-S-paracentral), parietal eye fields (S-intraparietal), thalamus, striatum (nigrotectal pathway) Horizontal saccadic eye movements: SN1 (SNr), sMRt (gigantocellular reticular nucleus), thalamus, cerebral cortex, caudate (basal ganglia; Quessy & Freedman, 2004) Motor function or pathway: ION, PBG, thalamus, cerebellum
Inferior colliculus (IC)	Auditory pathway: SOC, SN, thalamus, G-temp-sup-G-T-transv (auditory cortex), SC (May, 2006) Visual pathway: SC, S-calcarine (primary visual cortex)
Ventral tegmental area with parabrachial pigmented nucleus of the ventral tegmental area nuclei complex (VTA-PBP)	Motivated behaviors aversion (for VTA): medial prefrontal cortex, basal forebrain (bed nucleus of stria terminalis), hypothalamus, nucleus accumbens (Morales & Margolis, 2017) Reward (for VTA): LDTg, DR, basal forebrain (bed nucleus of stria terminalis and nucleus accumbens), hypothalamus, medial prefrontal cortex (Morales & Margolis, 2017), hippocampus, amygdala (Tang, Kochubey, Kintscher, & Schneggenburger, 2020) Arousal (for VTA): LC, DR, MnR, PTg, LDTg (Edlow et al., 2012) Mesostriatal and mesocortical pathways (for PBP): SN2 (SNc), basal forebrain (nucleus accumbens), prefrontal cortex Motor pathway (of VTA): Thalamus, cerebellum, supplementary motor area (Hosp et al., 2019)
Microcellular tegmental nucleus with parabigeminal nucleus (MiTg-PBG)	Visual stimulus and threat protection: SC, amygdala Retinogeniculocortical pathway: Thalamus Other pathways (e.g., autonomic/arousal): VSM (prepositus nucleus), LC, CnF, PAG and hypothalamus (Baleydier & Magnin, 1979)
Medial parabrachial nucleus (MPB)	Gustatory pathway: VSM (solitary nucleus), thalamus, S-circular insula inferior (primary taste cortex), S_orbital_medial-olfactory (septa-olfactory area), G-rectus, G-subcallosal (infralimbic cortex; Pritchard, 2012; Saper & Loewy, 1980), amygdala (bed nucleus of stria terminalis), hypothalamus
Lateral parabrachial nucleus (LPB)	Visceral pathway: VSM (solitary nucleus-caudal), amygdala, hypothalamus, basal forebrain (bed nucleus of stria terminalis), cerebral cortex (Fulwiler & Saper, 1984) Nociception: RMg
Vestibular nuclei complex (Ve)	Eye/head movement: ION, sMRt, cerebellum Balance: ION (which acts as a relay between Ve and the cerebellum), thalamus, insular cortex, cingulate cortex and cerebellum (Tellegen, Arends, & Dubbeldam, 2001) Sleep–wake state: LC, DR, LDTg-CGPn, PAG, SubC, PCRtA, PMnR, sMRt (gigantocellular reticular nucleus and lateral paragigantocellular nucleus; Kompotis et al., 2019) Emotional regulation: LC, DR, amygdala, insula Visceral pathway: LPB, VSM (solitary nucleus)
Superior olivary complex (SOC)	Auditory pathway: IC (Nieuwenhuys et al., 2008)
Superior medullary reticular formation (sMRt)	Eye movement pathway (of paragigantocellular nucleus): SC, cerebellum Medial somatic motor system (for gigantocellular nucleus): RMg, VSM (hypoglossal nerve nucleus), SC, Ve (head control), iMRt (ambiguus nucleus), and PAG (Holstege, 2009) Other (e.g., visceral, motor, limbic) pathway (of parvicellular reticular nucleus): PAG, VSM (vagus nerve nucleus, solitary nucleus, amygdala, hypothalamus (Blessing & Benarroch, 2012)
Inferior medullary reticular formation (iMRt)	Cardiovascular pathway (of ventral and dorsal medullary reticular nucleus): VSM (vagus nerve nucleus, solitary nucleus), hypothalamus Respiratory pathway (of ventral and dorsal medullary reticular nucleus): sMRt (paragigantocellular, parvocellular reticular nucleus) Respiratory pathway (of nucleus retroambiguus): LPB, VSM (solitary nucleus, hypoglossal nerve nucleus; Gerrits & Holstege, 1996), PAG (Holstege & Cowie, 1989) Nociceptive and associated motor reaction pathway (of dorsal medullary reticular nucleus): ION, VSM (solitary nucleus), sMRt, CnF, VTA, IC, LC, MPB, PAG, SN, thalamus, hypothalamus, pallidum, amygdala, cerebellum (Leite-Almeida, Valle-Fernandes, & Almeida, 2006)

TABLE 2 (Continued)

Brainstem nuclei	Connectivity
Viscerosensory motor nuclei complex (VSM)	Gustatory pathway (of solitary nucleus): medullary reticular formation nuclei (iMRt, sMRt), SOC, MPB, basal forebrain, amygdala, thalamus (Nieuwenhuys et al., 2008)
	Hypoglossal pathway (of hypoglossal nucleus, XII): parabrachial nuclei, RPa, ROb, VSM (solitary nucleus), sMRt (G. Holstege, 1991)
	Parasympathetic motor function (of vagus nerve nucleus, X): VSM (solitary nucleus), raphe nuclei, LC, medial prefrontal orbital cortex (the visceral motor cortex), amygdala, hypothalamus
Raphe magnus (RMg)	Intrinsic analgesia system and other non-nociceptive pathway): hypothalamus, PAG, sMRt (gigantocellular reticular nucleus pars alpha, parvocellular reticular nucleus), DR, mesencephalic reticular formation, LPB, LC, VSM (solitary nucleus), PnC, and medullary reticular formation (iMRt; sMRt; Beitz, 1982; Sim & Joseph, 1992)
	Pain pathway: PAG, LC (Sim & Joseph, 1992), LPB (G. Holstege, 1988)
Raphe pallidus (RPa)	Autonomic and somatic pathway: VSM (vagus nerve nucleus, hypoglossal nerve nucleus), parabrachial nuclei, SubC, sMRt, hypothalamus, basal forebrain, amygdala, insular cortex
	Motor control, respiratory and sympathetic regulation pathway: PAG, DR (Hermann et al., 1997)
Raphe obscurus (ROb)	Emotional motor and autonomic pathway: VSM (solitary nucleus), iMRt, sMRt, PAG (exerts affect as nociceptor), LDTg, PnO and LPB (Braz, Enquist, & Basbaum, 2009)
Parvicellular reticular nucleus-alpha part (PCRtA)	Autonomic regulation and orofacial motor control pathway: VSM (hypoglossal nerve nucleus and solitary nucleus), LPB, MPB, sMRt (gigantocellular reticular nucleus), raphe nuclei, ION (Ter Horst, Copray, Liem, & Van Willigen, 1991), mRt, SC, DR, SN1 (SNr), SubC, iMRt, hypothalamus, cerebellum (Shammah-Lagnado, Costa, & Ricardo, 1992)

rats (Leite-Almeida et al., 2006). We also found very strong connectivity with the thalamus, hypothalamus, pallidum, amygdala, and the cerebellar cortex. The retroambiguus nucleus is a multifunctional group of neurons involved in the output of the emotional motor system, such as vomiting, vocalization, mating, and changes in respiration (Subramanian, Huang, Silburn, Balnave, & Holstege, 2018). The periaqueductal gray (PAG)–nucleus retroambiguus (NRA) pathway has been shown to be involved in control of vocalization and sexual behavior and is evident by iMRt connectivity to PAG and amygdala here.

The **viscero-sensory-motor nuclei complex (VSM)** consists of solitary nucleus (Sol), vagus nerve nucleus (10N), hypoglossal nucleus (12N), prepositus (Pr), intercalated nucleus (In), and interpositus (IPo; Singh et al., 2021). Sol acts as an integration center for viscerosensory inputs. We observed connectivity of VSM with medullary reticular formation nuclei (iMRt, sMRt), parabrachial nuclei, thalamus and basal forebrain as expected for its role in respiration, cardiovascular response, nausea/vomiting, swallowing and taste (Nieuwenhuys et al., 2008; Saper & Stornetta, 2015). 12N also receives inputs from RPa, ROb (Manaker & Tischler, 1993) as found in our connectome. 10N has connections with amygdala, hypothalamus, basal forebrain, RPa, RMg, ROb (Tache, 2012), and Sol and LC (Chen & Williams, 2012) for autonomic functions and mediation of memory from stressful situations respectively. We found links of VSM with these regions in the human connectome.

The **raphe magnus (RMg)** is involved in pain modulation and regulation of reflexive emotional responses (Hornung, 2012). It showed expected structural connectivity to the sMRt (magnocellular reticular nucleus; Leanza, Perez, Pellitteri, Russo, & Stanzani, 1995), hypothalamus, PAG, LC, parabrachial nucleus and solitary tract (included in VSM in our human connectome; Sim & Joseph, 1992), bed nucleus of stria terminalis (amygdala), and preoptic area (hypothalamus; G. Holstege, 1991; G. G. Holstege, Mouton, & Gerrits, 2004; Figure 7b).

Raphe pallidus (RPa) is the smallest raphe nucleus in the brain. It sends efferents to the spinal cord and motor nuclei (trigeminal, facial dorsal motor vagal, hypoglossal, included in the VSM) and receives afferents from anterolateral hypothalamus and PAG (Hermann, Luppi, Peyron, Hinckel, & Jouvet, 1996; Hermann et al., 1997; G. Holstege, 1991). It also receives small/moderate afferents from lateral preoptic area, bed nucleus of stria terminalis, paraventricular hypothalamic nucleus, amygdala, parabrachial nuclei, SubC, PCRtA, insular, and perirhinal cortices (Tanaka et al., 1994). In our human connectome, in line with these findings, we observed connectivity of RPa with PAG, VSM, hypothalamus, basal forebrain, amygdala, LPB, MPB, SubC, PCRtA.

The **raphe obscurus (ROb)** is the caudal part of the limbic system and of the emotional motor system (G. G. Holstege et al., 2004). It sends efferents to the spinal cord and cerebellum and connects autonomic and somatosensory motor neurons. It also provides modulatory serotonergic input to brainstem motor nuclei such as nucleus accumbens and pre-Boetzinger (Saper & Stornetta, 2015). Projections from ROb affecting the autonomic dorsal vagal complex terminate in the solitary nucleus, part of VSM in our human study (Weissheimer &

Machado, 2007). Consistent with neuroanatomical studies, it showed connectivity with the medullary reticular formation (iMRt and sMRt; Braz et al., 2009) and Ve (Halberstadt & Balaban, 2003). We also found structural connectivity of ROb with LDTg, PnO, and LPB, indicating its involvement in modulating emotional and autonomic processes (Figure 8b).

Parvicellular reticular nucleus-alpha part (PCRtA) is the alpha part of the parvicellular reticular nucleus described in Paxinos et al. (2012). There is paucity of studies commenting on its location and function. The parvicellular reticular nucleus (non-alpha part) is part of sMRt nucleus as described above. It is involved in motor, autonomic (cardiovascular and visceral), and reflexive emotional functions. The PCRtA showed connectivity with limbic structures of basal forebrain, amygdala, hypothalamus and PAG (G. Holstege, 2014). It also showed connectivity with amygdala, hypothalamus, VSM (including solitary nucleus, X and XII nuclei), RN1, RN2, SNr, SC, LPB, MPB, sMRt, and iMRt (intermediate reticular nucleus; Shammah-Lagnado et al., 1992; Ter Horst et al., 1991).

4.2 | Graph analysis

Looking at nodal graph measure, we found above average degree centrality values for VTA-PBP, LPB, MPB, PCRtA, sMRt, iMRt, RPa, and ROb. These nuclei along with MiTg-PBG, Ve, SOC, RMg also showed above average values of normalized participant coefficient. These findings support our current hypothesis of involvement of these nuclei communicating between to autonomic/limbic/nociceptive network, and autonomic–vestibular network. As postulated, these nuclei emerged as "hubs" in networks showing strong connectivity with other regions. Also, they exhibited connectivity between their own community and the other communities operating as part of a circuit.

4.3 | Clinical translation of the current work

We found good association and percentage of common links between 7 Tesla and 3 Tesla data in whole brain targets, brainstem only targets, cortical/other subcortical targets, thereby indicating translation of our high-resolution structural connectome at 7 Tesla to clinical resolution data at 3 Tesla. The percentage of common links decreased steeply with increasing the statistical threshold, especially for the cortex/subcortex and to a lesser extent for the brainstem. This demonstrates more robust translatability for structural connectivity within brainstem nuclei than of brainstem nuclei with cortical/subcortical areas, possibly due to the inherent increased sensitivity of the tractography technique to proximal than distal regions. The nuclei studied in the current work are involved in maintenance of vital autonomic functions and are relevant for diseases of both children and adults. For example, sMRt, iMRt, ROb, and VSM have been widely studied in sudden infant death syndrome (SIDS) in children under 12 months of age (Kinney & Haynes, 2019). We foresee extension of our current atlas and connectome methodology to children to better understand this enigmatic condition. In diseases where these nuclei overlap in function and their involvement in specific pathophysiologic processes is unclear (e.g., SN and VTA-PBP in Parkinson's disease), this atlas may elucidate their role in inception and progression of disease. In situations where these nuclei are neighboring and modulate each other's activity, they can be studied as single entity like the VSM complex (Singh et al., 2021). This nuclei complex has recently been proposed to underlie stress related disorders, brain–gut health, hypertension, and SIDS (Breit, Kupferberg, Rogler, & Hasler, 2018; Holsboer, 2000; Mancia & Grassi, 2014; Sanvictores & Tadi, 2021).

4.4 | Circuit diagram

Seeds and targets were grouped, according to their function in (a) an autonomic/limbic/nociceptive diagram, (b) a vestibular diagram, and (c) a diagram of autonomic–vestibular interactions. In circuit (a) the nuclei of VTA-PBP, CLi-RLi, PAG, LPB, MPB, PCRtA, RMg, RPa, ROb, sMRt, VSM, and iMRt showed connectivity among themselves, with cerebellum, cortical, and subcortical structures. VTA-PBP connections were seen with limbic, autonomic and nociception associated regions of anterior cingulate cortex, infralimbic cortex, orbitofrontal cortex, accumbens area, anterior insula, amygdala, hypothalamus, PAG and raphe nuclei. In the vestibular circuit (b), the vestibular nucleus acted as the pivotal nucleus, which connected to cerebellum, cortical and subcortical regions involved in vestibular function (see Section 2 for regions list). The ION, involved in this circuitry, connected to vestibular nuclei, and the latter connected to cerebellum thus showing connections of the vestibulo-olivary-cerebellar pathway (Sugihara & Shinoda, 2004). As expected, the ION connected to the Ve nuclei, hippocampus, and thalamus. Interestingly, nuclei involved in autonomic functions displayed connectivity with vestibular nuclei (see the autonomic–vestibular circuit), specifically Ve showed connectivity to cerebellum, cortical (anterior cingulate, infralimbic, and orbitofrontal cortex) and subcortical regions (amygdala, insula, hypothalamus, and accumbens), thus identifying Ve as relay center for modulating interactions within autonomic regions. This is relevant for chronic vestibular disorders, in which adverse vestibular-autonomic/limbic interactions (Brandt, 1996; Bronstein, 2004; Indovina et al., 2015; Jacob et al., 2009; Staab, 2012; Staab et al., 2017, 2014) seem to play a role in determining the success of compensatory processes in the recovery of patients from acute vestibular deficits.

4.5 | Strengths and limitations of current study

The current work is based on a high-resolution brainstem probabilistic structural atlas derived from living humans developed at 7 Tesla and automatically aligned to in vivo diffusion-based MRI. This approach is faster and more precise than performing manual/visual extrapolation from ex vivo atlases. In this work, we used a custom-built 32-channel receive coil and volume transmit coil at 7 Tesla, which provided enhanced sensitivity and higher spatial resolution in the deeper

brainstem regions for the diffusion dataset. This provided enhanced precision for alignment of the brainstem nuclei atlas to high-angular resolution diffusion dataset. Also, the current work gained strength from demonstrating good translatability of brainstem connectomic results to clinical resolution datasets acquired at 3 Tesla. Moreover, the sample size ($n = 19$) was sufficient to provide significant results after necessary corrections for multiple comparisons.

We acknowledge methodological limitations of this work. Despite continuous improvements, diffusion-based tractography is unable to detangle fiber crossing and cannot distinguish efferent from afferent connections and direct from indirect connectivity. Moreover, larger fibers are easier to map than smaller fiber bundles, and streamline probability increases near the seed region compared to distant locations. This might have introduced spurious links into the results. Further work using more recent methods based on anatomically constrained tractography and spherical deconvolution informed filtering of tractograms might improve connectomes by constraining false positives and negatives. Their use would also expand the graph-based network analysis by enabling the inclusion of more parameters extracted from the full square connectivity matrix. Nevertheless, the absence of a precise definition of gray matter and white matter masks in the brainstem is a limitation, which must be overcome for the proper application of these alternative anatomically constrained tractography techniques to the brainstem.

Another limitation of structural connectomes based on diffusion tractography is the lack of a consensus on the thresholding method (Buchanan et al., 2020). As opposed to absolute- or density-thresholding, we applied thresholding based on group level statistics, which assumes that connections with the highest intersubject variability are spurious. The relatively small sample size did not allow us to apply Bonferroni correction for multiple comparisons to the connectome results, yet we were able to use a conservative ($p < .0005$) FDR correction. Thus, despite good reproducibility of our results across scanners, we acknowledge that future tractography and histological/tract-tracing studies are warranted to demonstrate reproducibility and further validate our results, as anatomically plausible measures of connectivity.

4.6 | Conclusion

This comprehensive investigation examined the structural connectivity of human autonomic, pain, limbic, and sensory brainstem nuclei in vivo using a high-resolution probabilistic brainstem nuclei atlas and diffusion imaging at 7 Tesla and 3 Tesla. This study adds to existing knowledge of structural connectivity of brainstem nuclei involved in multiple functions, and demonstrated the feasibility of mapping the connections among nodes in a manner consistent with known neuroanatomical and neurophysiological connectivity. The current work also demonstrated its translatability into datasets obtained with usual resolution thereby paving the way for clinical applications studying functional and structural abnormalities in disease conditions relating to these nuclei.

CONFLICT OF INTEREST

The authors declare no conflicts of interest.

ETHICS STATEMENT

The study was conducted according to the guidelines of the declaration of Helsinki and approved by the Massachusetts General Hospital Institutional Review Board. All participants gave written informed consent prior to participation.

DATA AVAILABILITY STATEMENT

Connectivity data will be shared by request from any qualified investigator.

ORCID

Kavita Singh https://orcid.org/0000-0002-4772-372X
María Guadalupe García-Gomar https://orcid.org/0000-0001-5633-3419

REFERENCES

Aitkin, L. (1979). The auditory midbrain. *Trends in Neurosciences*, *2*, 308–310. https://doi.org/10.1016/0166-2236(79)90119-X

Balaban, C. D. (2004). Projections from the parabrachial nucleus to the vestibular nuclei: Potential substrates for autonomic and limbic influences on vestibular responses. *Brain Research*, *996*(1), 126–137.

Baleydier, C., & Magnin, M. (1979). Afferent and efferent connections of the parabigeminal nucleus in cat revealed by retrograde axonal transport of horseradish peroxidase. *Brain Research*, *161*(2), 187–198. https://doi.org/10.1016/0006-8993(79)90062-3

Beitz, A. J. (1982). The organization of afferent projections to the midbrain periaqueductal gray of the rat. *Neuroscience*, *7*(1), 133–159. https://doi.org/10.1016/0306-4522(82)90157-9

Bianciardi, M., Strong, C., Toschi, N., Edlow, B. L., Fischl, B., Brown, E. N., … Wald, L. L. (2018). A probabilistic template of human mesopontine tegmental nuclei from in vivo 7 T MRI. *NeuroImage*, *170*, 222–230. https://doi.org/10.1016/j.neuroimage.2017.04.070

Bianciardi, M., Toschi, N., Edlow, B. L., Eichner, C., Setsompop, K., Polimeni, J. R., … Wald, L. L. (2015). Toward an in vivo neuroimaging template of human brainstem nuclei of the ascending arousal, autonomic, and motor systems. *Brain Connectivity*, *5*(10), 597–607. https://doi.org/10.1089/brain.2015.0347

Bianciardi, M., Toschi, N., Eichner, C., Polimeni, J. R., Setsompop, K., Brown, E. N., … Wald, L. L. (2016). In vivo functional connectome of human brainstem nuclei of the ascending arousal, autonomic, and motor systems by high spatial resolution 7-Tesla fMRI. *Magma*, *29*(3), 451–462. https://doi.org/10.1007/s10334-016-0546-3

Bickford, M. E., Ramcharan, E., Godwin, D. W., Erişir, A., Gnadt, J., & Sherman, S. M. (2000). Neurotransmitters contained in the subcortical extraretinal inputs to the monkey lateral geniculate nucleus. *The*

Journal of Comparative Neurology, 424(4), 701–717. https://doi.org/10.1002/1096-9861(20000904)424:4<701::aid-cne11>3.0.co;2-b

Blessing, W. W., & Benarroch, E. E. (2012). Chapter 29—Lower brainstem regulation of visceral, cardiovascular, and respiratory function. In J. K. Mai & G. Paxinos (Eds.), *The human nervous system* (3rd ed., pp. 1058–1073). San Diego, CA: Academic Press. https://doi.org/10.1016/B978-0-12-374236-0.10029-X

Brandt, T. (1996). Phobic postural vertigo. *Neurology, 46*(6), 1515–1519. https://doi.org/10.1212/WNL.46.6.1515

Brandt, T., & Dieterich, M. (2019). Thalamocortical network: A core structure for integrative multimodal vestibular functions. *Current Opinion in Neurology, 32*(1), 154–164. https://doi.org/10.1097/WCO.0000000000000638

Braz, J. M., Enquist, L. W., & Basbaum, A. I. (2009). Inputs to serotonergic neurons revealed by conditional viral transneuronal tracing. *The Journal of Comparative Neurology, 514*(2), 145–160. https://doi.org/10.1002/cne.22003

Breit, S., Kupferberg, A., Rogler, G., & Hasler, G. (2018). Vagus nerve as modulator of the brain–gut axis in psychiatric and inflammatory disorders. *Frontiers in Psychiatry, 9*, 44. https://doi.org/10.3389/fpsyt.2018.00044

Bronstein, A. M. (2004). Vision and vertigo. *Journal of Neurology, 251*(4), 381–387. https://doi.org/10.1007/s00415-004-0410-7

Buchanan, C. R., Bastin, M. E., Ritchie, S. J., Liewald, D. C., Madole, J. W., Tucker-Drob, E. M., ... Cox, S. R. (2020). The effect of network thresholding and weighting on structural brain networks in the UKbiobank. *NeuroImage, 211*, 116443. https://doi.org/10.1016/j.neuroimage.2019.116443

Bullmore, E., & Sporns, O. (2009). Complex brain networks: Graph theoretical analysis of structural and functional systems. *Nature Reviews Neuroscience, 10*(3), 186–198. https://doi.org/10.1038/nrn2575

Chamberlin, N. L., & Saper, C. B. (1995). Differential distribution of AMPA-selective glutamate receptor subunits in the parabrachial nucleus of the rat. *Neuroscience, 68*(2), 435–443. https://doi.org/10.1016/0306-4522(95)00129-7

Chen, C. C., & Williams, C. L. (2012). Interactions between epinephrine, ascending vagal fibers, and central noradrenergic systems in modulating memory for emotionally arousing events. *Frontiers in Behavioral Neuroscience, 6*, 35. https://doi.org/10.3389/fnbeh.2012.00035

Chuhma, N., Mingote, S., Moore, H., & Rayport, S. (2014). Dopamine neurons control striatal cholinergic neurons via regionally heterogeneous dopamine and glutamate signaling. *Neuron, 81*(4), 901–912. https://doi.org/10.1016/j.neuron.2013.12.027

Cohen, B., & Büttner-Ennever, J. A. (1984). Projections from the superior colliculus to a region of the central mesencephalic reticular formation (cMRF) associated with horizontal saccadic eye movements. *Experimental Brain Research, 57*(1), 167–176. https://doi.org/10.1007/BF00231143

Coleman, J. R., & Clerici, W. J. (1987). Sources of projections to subdivisions of the inferior colliculus in the rat. *The Journal of Comparative Neurology, 262*(2), 215–226. https://doi.org/10.1002/cne.902620204

Coomes, D. L., & Schofield, B. R. (2004). Projections from the auditory cortex to the superior olivary complex in Guinea pigs. *The European Journal of Neuroscience, 19*(8), 2188–2200. https://doi.org/10.1111/j.0953-816X.2004.03317.x

Cowie, R. J., & Robinson, D. L. (1994). Subcortical contributions to head movements in macaques. I. Contrasting effects of electrical stimulation of a medial pontomedullary region and the superior colliculus. *Journal of Neurophysiology, 72*(6), 2648–2664. https://doi.org/10.1152/jn.1994.72.6.2648

Datta, S., Curró Dossi, R., Paré, D., Oakson, G., & Steriade, M. (1991). Substantia nigra reticulata neurons during sleep-waking states: Relation with ponto-geniculo-occipital waves. *Brain Research, 566*(1–2), 344–347. https://doi.org/10.1016/0006-8993(91)91723-e

Deichler, A., Carrasco, D., Lopez-Jury, L., Vega-Zuniga, T., Márquez, N., Mpodozis, J., & Marín, G. J. (2020). A specialized reciprocal connectivity suggests a link between the mechanisms by which the superior colliculus and parabigeminal nucleus produce defensive behaviors in rodents. *Scientific Reports, 10*(1), 16220. https://doi.org/10.1038/s41598-020-72848-0

Desikan, R. S., Ségonne, F., Fischl, B., Quinn, B. T., Dickerson, B. C., Blacker, D., ... Killiany, R. J. (2006). An automated labeling system for subdividing the human cerebral cortex on MRI scans into gyral based regions of interest. *NeuroImage, 31*(3), 968–980. https://doi.org/10.1016/j.neuroimage.2006.01.021

Dessem, D., & Luo, P. (1999). Jaw-muscle spindle afferent feedback to the cervical spinal cord in the rat. *Experimental Brain Research, 128*(4), 451–459. https://doi.org/10.1007/s002210050868

Destrieux, C., Fischl, B., Dale, A., & Halgren, E. (2010). Automatic parcellation of human cortical gyri and sulci using standard anatomical nomenclature. *NeuroImage, 53*(1), 1–15. https://doi.org/10.1016/j.neuroimage.2010.06.010

Eban-Rothschild, A., Rothschild, G., Giardino, W. J., Jones, J. R., & de Lecea, L. (2016). VTA dopaminergic neurons regulate ethologically relevant sleep-wake behaviors. *Nature Neuroscience, 19*(10), 1356–1366. https://doi.org/10.1038/nn.4377

Edlow, B. L., Takahashi, E., Wu, O., Benner, T., Dai, G., Bu, L., ... Folkerth, R. D. (2012). Neuroanatomic connectivity of the human ascending arousal system critical to consciousness and its disorders. *Journal of Neuropathology and Experimental Neurology, 71*(6), 531–546. https://doi.org/10.1097/NEN.0b013e3182588293

Eickhoff, S. B., Stephan, K. E., Mohlberg, H., Grefkes, C., Fink, G. R., Amunts, K., & Zilles, K. (2005). A new SPM toolbox for combining probabilistic cytoarchitectonic maps and functional imaging data. *NeuroImage, 25*(4), 1325–1335. https://doi.org/10.1016/j.neuroimage.2004.12.034

Englot, D. J., Gonzalez, H. F. J., Reynolds, B. B., Konrad, P. E., Jacobs, M. L., Gore, J. C., ... Morgan, V. L. (2018). Relating structural and functional brainstem connectivity to disease measures in epilepsy. *Neurology, 91*(1), e67–e77. https://doi.org/10.1212/WNL.0000000000005733

Fan, L., Li, H., Zhuo, J., Zhang, Y., Wang, J., Chen, L., ... Jiang, T. (2016). The human Brainnetome atlas: A new brain atlas based on connectional architecture. *Cerebral Cortex, 26*(8), 3508–3526. https://doi.org/10.1093/cercor/bhw157

Fay, R. R., Popper, A. N., & Webster, D. B. (1992). *The mammalian auditory pathway: Neuroanatomy.* New York: Springer-Verlag.

Frackowiak, R. S. J., Ashburner, J. T., Penny, W. D., & Zeki, S. (2004). In K. J. Friston, C. D. Frith, R. J. Dolan, & C. J. Price (Eds.), *Human brain function* (2nd ed.). San Diego, CA: Academic Press.

Fulwiler, C. E., & Saper, C. B. (1984). Subnuclear organization of the efferent connections of the parabrachial nucleus in the rat. *Brain Research, 319*(3), 229–259. https://doi.org/10.1016/0165-0173(84)90012-2

García-Gomar, M. G., Singh, K., & Bianciardi, M. (2021). *Probabilistic structural atlas and connectome of brainstem nuclei involved in arousal and sleep by 7 Tesla MRI in living humans.* Paper presented at ISMRM 29th Annual Meeting & Exhibition.

García-Gomar, M. G., Strong, C., Toschi, N., Singh, K., Rosen, B. R., Wald, L. L., & Bianciardi, M. (2019). In vivo probabilistic structural atlas of the inferior and superior colliculi, medial and lateral geniculate nuclei and superior olivary complex in humans based on 7 Tesla MRI. *Frontiers in Neuroscience, 13*, 764. https://doi.org/10.3389/fnins.2019.00764

García-Gomar, M. G., Videnovic, A., Singh, K., Stauder, M., Lewis, L. D., Wald, L. L., ... Bianciardi, M. (2021). Disruption of brainstem structural connectivity in REM sleep behavior disorder using 7 Tesla magnetic resonance imaging. *Movement Disorders, 37*(4), 847–853. https://doi.org/10.1002/mds.28895

Gerrits, P. O., & Holstege, G. (1996). Pontine and medullary projections to the nucleus retroambiguus: a wheat germ agglutinin-horseradish peroxidase and autoradiographic tracing study in the cat. *J Comp Neurol, 16*(373(2)), 173–185.

Gerrits, P. O., Mouton, L. J., de Weerd, H., Georgiadis, J. R., Krukerink, M., & Holstege, G. (2004). Ultrastructural evidence for a

direct excitatory pathway from the nucleus retroambiguus to lateral longissimus and quadratus lumborum motoneurons in the female golden hamster. *The Journal of Comparative Neurology*, 480(4), 352–363. https://doi.org/10.1002/cne.20366

Goldberg, J. M., Wilson, V. J., Cullen, K. E., Angelaki, D. E., Broussard, D. M., Buttner-Ennever, J., ... Minor, L. B. (2012). *The vestibular system: A sixth sense* (1st ed.). New York, NY: Oxford University Press.

Grabner, G., Janke, A. L., Budge, M. M., Smith, D., Pruessner, J., & Collins, D. L. (2006). Symmetric atlasing and model based segmentation: An application to the hippocampus in older adults. *Medical Image Computing and Computer-Assisted Intervention*, 9(Pt 2), 58–66. https://doi.org/10.1007/11866763_8

Halberstadt, A. L., & Balaban, C. D. (2003). Organization of projections from the raphe nuclei to the vestibular nuclei in rats. *Neuroscience*, 120(2), 573–594. https://doi.org/10.1016/S0306-4522(02)00952-1

Halliday, G., Reyes, S., & Double, K. (2012). Chapter 13—Substantia Nigra, ventral tegmental area, and Retrorubral fields. In J. K. Mai & G. Paxinos (Eds.), *The human nervous system* (3rd ed., pp. 439–455). San Diego, CA: Academic Press. https://doi.org/10.1016/B978-0-12-374236-0.10013-6

Harper, R. M., Kumar, R., Ogren, J. A., & Macey, P. M. (2013). Sleep-disordered breathing: Effects on brain structure and function. *Respiratory Physiology & Neurobiology*, 188(3), 383–391. https://doi.org/10.1016/j.resp.2013.04.021

Harting, J. K., & Updyke, B. V. (2006). Oculomotor-related pathways of the basal ganglia. *Progress in Brain Research*, 151, 441–460. https://doi.org/10.1016/S0079-6123(05)51014-8

Harting, J. K., van Lieshout, D. P., & Feig, S. (1991). Connectional studies of the primate lateral geniculate nucleus: Distribution of axons arising from the thalamic reticular nucleus of *Galago crassicaudatus*. *Journal of Comparative Neurology*, 310(3), 411–427. https://doi.org/10.1002/cne.903100310

Hermann, D. M., Luppi, P. H., Peyron, C., Hinckel, P., & Jouvet, M. (1996). Forebrain projections of the rostral nucleus raphe magnus shown by iontophoretic application of choleratoxin b in rats. *Neuroscience Letters*, 216(3), 151–154. https://doi.org/10.1016/0304-3940(96)13013-5

Hermann, D. M., Luppi, P. H., Peyron, C., Hinckel, P., & Jouvet, M. (1997). Afferent projections to the rat nuclei raphe magnus, raphe pallidus and reticularis gigantocellularis pars alpha demonstrated by iontophoretic application of choleratoxin (subunit b). *Journal of Chemical Neuroanatomy*, 13(1), 1–21. https://doi.org/10.1016/s0891-0618(97)00019-7

Holsboer, F. (2000). The corticosteroid receptor hypothesis of depression. *Neuropsychopharmacology*, 23(5), 477–501. https://doi.org/10.1016/S0893-133X(00)00159-7

Holstege, G. (1988). Anatomical evidence for a strong ventral parabrachial projection to nucleus raphe magnus and adjacent tegmental field. *Brain Research*, 447(1), 154–158. https://doi.org/10.1016/0006-8993(88)90977-8

Holstege, G., & Cowie, R. J. (1989). Projections from the rostral mesencephalic reticular formation to the spinal cord. *Experimental Brain Research*, 75(2). https://doi.org/10.1007/bf00247933

Holstege, G. (1991). Descending motor pathways and the spinal motor system: Limbic and non-limbic components. *Progress in Brain Research*, 87, 307–421. https://doi.org/10.1016/s0079-6123(08)63057-5

Holstege, G. (2009). The mesopontine rostromedial tegmental nucleus and the emotional motor system: Role in basic survival behavior. *The Journal of Comparative Neurology*, 513(6), 559–565. https://doi.org/10.1002/cne.21990

Holstege, G. (2014). The periaqueductal gray controls brainstem emotional motor systems including respiration. *Progress in Brain Research*, 209, 379–405. https://doi.org/10.1016/B978-0-444-63274-6.00020-5

Holstege, G., Georgiadis, J. R., Paans, A. M. J., Meiners, L. C., van der Graaf, F. H. C. E., & Reinders, A. A. T. S. (2003). Brain activation during human male ejaculation. *Journal of Neuroscience*, 23(27), 9185–9193.

Holstege, G. G., Mouton, L. J., & Gerrits, P. O. (2004). CHAPTER 36—Emotional motor system. In G. Paxinos & J. K. Mai (Eds.), *The human nervous system* (2nd ed., pp. 1306–1324). San Diego, CA: Academic Press. https://doi.org/10.1016/B978-012547626-3/50037-5

Horn, A. K. E. (2006). The reticular formation. *Progress in Brain Research*, 151, 127–155. https://doi.org/10.1016/S0079-6123(05)51005-7

Hornung, J.-P. (2003). The human raphe nuclei and the serotonergic system. *Journal of Chemical Neuroanatomy*, 26(4), 331–343. https://doi.org/10.1016/j.jchemneu.2003.10.002

Hornung, J.-P. (2012). Chapter 11—Raphe nuclei. In J. K. Mai & G. Paxinos (Eds.), *The human nervous system* (3rd ed., pp. 401–424). San Diego, CA: Academic Press. https://doi.org/10.1016/B978-0-12-374236-0.10011-2

Hosp, J. A., Coenen, V. A., Rijntjes, M., Egger, K., Urbach, H., Weiller, C., & Reisert, M. (2019). Ventral tegmental area connections to motor and sensory cortical fields in humans. *Brain Structure & Function*, 224(8), 2839–2855. https://doi.org/10.1007/s00429-019-01939-0

Huerta, M. F., & Kaas, J. H. (1990). Supplementary eye field as defined by intracortical microstimulation: Connections in macaques. *The Journal of Comparative Neurology*, 293(2), 299–330. https://doi.org/10.1002/cne.902930211

Huerta, M. F., Krubitzer, L. A., & Kaas, J. H. (1986). Frontal eye field as defined by intracortical microstimulation in squirrel monkeys, owl monkeys, and macaque monkeys: I. subcortical connections. *The Journal of Comparative Neurology*, 253(4), 415–439. https://doi.org/10.1002/cne.902530402

Ikemoto, S., & Wise, R. A. (2004). Mapping of chemical trigger zones for reward. *Neuropharmacology*, 47, 190–201. https://doi.org/10.1016/j.neuropharm.2004.07.012

Indovina, I., Bosco, G., Riccelli, R., Maffei, V., Lacquaniti, F., Passamonti, L., & Toschi, N. (2020). Structural connectome and connectivity lateralization of the multimodal vestibular cortical network. *NeuroImage*, 222, 117247. https://doi.org/10.1016/j.neuroimage.2020.117247

Indovina, I., Riccelli, R., Chiarella, G., Petrolo, C., Augimeri, A., Giofrè, L., ... Passamonti, L. (2015). Role of the insula and vestibular system in patients with chronic subjective dizziness: An fMRI study using sound-evoked vestibular stimulation. *Frontiers in Behavioral Neuroscience*, 9, 334. https://doi.org/10.3389/fnbeh.2015.00334

Irimia, A., Chambers, M. C., Torgerson, C. M., & Van Horn, J. D. (2012). Circular representation of human cortical networks for subject and population-level connectomic visualization. *NeuroImage*, 60(2), 1340–1351. https://doi.org/10.1016/j.neuroimage.2012.01.107

Jacob, R. G., Redfern, M. S., & Furman, J. M. (2009). Space and motion discomfort and abnormal balance control in patients with anxiety disorders. *Journal of Neurology, Neurosurgery & Psychiatry*, 80(1), 74–78. https://doi.org/10.1136/jnnp.2007.136432

Kaur, S., Wang, J. L., Ferrari, L., Thankachan, S., Kroeger, D., Venner, A., ... Saper, C. B. (2017). A genetically-defined circuit for arousal from sleep during hypercapnia. *Neuron*, 96(5), 1153–1167.e5. https://doi.org/10.1016/j.neuron.2017.10.009

Keil, B., Blau, J. N., Biber, S., Hoecht, P., Tountcheva, V., Setsompop, K., ... Wald, L. L. (2013). A 64-channel 3T array coil for accelerated brain MRI. *Magnetic Resonance in Medicine*, 70(1), 248–258. https://doi.org/10.1002/mrm.24427

Kinney, H. C., & Haynes, R. L. (2019). The serotonin brainstem hypothesis for the sudden infant death syndrome. *Journal of Neuropathology and Experimental Neurology*, 78(9), 765–779. https://doi.org/10.1093/jnen/nlz062

Kompotis, K., Hubbard, J., Emmenegger, Y., Perrault, A., Mühlethaler, M., Schwartz, S., ... Franken, P. (2019). Rocking promotes sleep in mice through rhythmic stimulation of the vestibular system. *Current Biology*, 29(3), 392–401.e4. https://doi.org/10.1016/j.cub.2018.12.007

Lacalle, S., & Saper, C. B. (2000). Calcitonin gene-related peptide-like immunoreactivity marks putative visceral sensory pathways in human

brain. *Neuroscience*, *100*, 115–130. https://doi.org/10.1016/S0306-4522(00)00245-1

Leanza, G., Perez, S., Pellitteri, R., Russo, A., & Stanzani, S. (1995). Branching serotonergic and non-serotonergic projections from caudal brainstem to the medial preoptic area and the lumbar spinal cord, in the rat. *Neuroscience Letters*, *200*(1), 5–8. https://doi.org/10.1016/0304-3940(95)12068-f

Lee, J., & Groh, J. M. (2012). Auditory signals evolve from hybrid- to eye-centered coordinates in the primate superior colliculus. *Journal of Neurophysiology*, *108*(1), 227–242. https://doi.org/10.1152/jn.00706.2011

Leite-Almeida, H., Valle-Fernandes, A., & Almeida, A. (2006). Brain projections from the medullary dorsal reticular nucleus: An anterograde and retrograde tracing study in the rat. *Neuroscience*, *140*(2), 577–595. https://doi.org/10.1016/j.neuroscience.2006.02.022

Lima, M. M. S., Andersen, M. L., Reksidler, A. B., Vital, M. A. B. F., & Tufik, S. (2007). The role of the substantia nigra pars compacta in regulating sleep patterns in rats. *PLoS One*, *2*(6), e513. https://doi.org/10.1371/journal.pone.0000513

Lima, M. M. S., Reksidler, A. B., & Vital, M. A. B. F. (2008). The dopaminergic dilemma: Sleep or wake? Implications in Parkinson's disease. *Bioscience Hypotheses*, *1*(1), 9–13. https://doi.org/10.1016/j.bihy.2008.01.010

Loewy, A. D., & Neil, J. J. (1981). The role of descending monoaminergic systems in central control of blood pressure. *Federation Proceedings*, *40*(13), 2778–2785.

Manaker, S., & Tischler, L. J. (1993). Origin of serotoninergic afferents to the hypoglossal nucleus in the rat. *The Journal of Comparative Neurology*, *334*(3), 466–476. https://doi.org/10.1002/cne.903340310

Mancia, G., & Grassi, G. (2014). The autonomic nervous system and hypertension. *Circulation Research*, *114*(11), 1804–1814. https://doi.org/10.1161/CIRCRESAHA.114.302524

Manjón, J. V., Coupé, P., Concha, L., Buades, A., Collins, D. L., & Robles, M. (2013). Diffusion weighted image denoising using overcomplete local PCA. *PLoS One*, *8*(9), e73021. https://doi.org/10.1371/journal.pone.0073021

May, P. J. (2006). The mammalian superior colliculus: Laminar structure and connections. *Progress in Brain Research*, *151*, 321–378. https://doi.org/10.1016/S0079-6123(05)51011-2

Mellott, J. G., Beebe, N. L., & Schofield, B. R. (2018). GABAergic and non-GABAergic projections to the superior colliculus from the auditory brainstem. *Brain Structure & Function*, *223*(4), 1923–1936. https://doi.org/10.1007/s00429-017-1599-4

Mena-Segovia, J. (2016). Structural and functional considerations of the cholinergic brainstem. *Journal of Neural Transmission*, *123*(7), 731–736. https://doi.org/10.1007/s00702-016-1530-9

Merel, J., Botvinick, M., & Wayne, G. (2019). Hierarchical motor control in mammals and machines. *Nature Communications*, *10*(1), 5489. https://doi.org/10.1038/s41467-019-13239-6

Moga, M. M., Saper, C. B., & Gray, T. S. (1990). Neuropeptide organization of the hypothalamic projection to the parabrachial nucleus in the rat. *The Journal of Comparative Neurology*, *295*(4), 662–682. https://doi.org/10.1002/cne.902950409

Morales, M., & Margolis, E. B. (2017). Ventral tegmental area: Cellular heterogeneity, connectivity and behaviour. *Nature Reviews Neuroscience*, *18*(2), 73–85. https://doi.org/10.1038/nrn.2016.165

Morgane, P. J., Galler, J. R., & Mokler, D. J. (2005). A review of systems and networks of the limbic forebrain/limbic midbrain. *Progress in Neurobiology*, *75*(2), 143–160. https://doi.org/10.1016/j.pneurobio.2005.01.001

Morikawa, H., & Paladini, C. A. (2011). Dynamic regulation of midbrain dopamine neuron activity: Intrinsic, synaptic, and plasticity mechanisms. *Neuroscience*, *198*, 95–111. https://doi.org/10.1016/j.neuroscience.2011.08.023

Moruzzi, G., & Magoun, H. W. (1949). Brain stem reticular formation and activation of the EEG. *Electroencephalography and Clinical Neurophysiology*, *1*(4), 455–473.

Naidich, T. P., Duvernoy, H. M., Delman, B. N., Sorensen, A. G., Kollias, S. S., & Haacke, E. M. (2009). *Duvernoy's atlas of the human brain stem and cerebellum: High-field MRI, surface anatomy, internal structure, vascularization and 3D sectional anatomy*. Austria: Springer Science & Business Media.

Nieuwenhuys, R., Voogd, J., & Van Huijzen, C. (2008). *The human central nervous system: A synopsis and atlas* (4th ed.). Springer: Berlin. https://doi.org/10.1007/978-3-540-34686-9

Olszewski, J., & Baxter, D. (1954). Cytoarchitecture of the human brain stem. Retrieved from https://www.cabdirect.org/cabdirect/abstract/19562201844

Olszewski, G., & Baxter, D. W. (2014). In J. A. Büttner-Ennever & A. K. E. Horn (Eds.), *Olszewski and Baxter's cytoarchitecture of the human brainstem*. North America: Karger.

Parvizi, J., & Damasio, A. (2001). Consciousness and the brainstem. *Cognition*, *79*(1–2), 135–160. https://doi.org/10.1016/s0010-0277(00)00127-x

Pauli, W. M., Nili, A. N., & Tyszka, J. M. (2018). A high-resolution probabilistic in vivo atlas of human subcortical brain nuclei. *Scientific Data*, *5*, 180063. https://doi.org/10.1038/sdata.2018.63

Paxinos, G., & Huang, X.-F. (1995). Atlas of the human brain stem. Faculty of Health and Behavioural Sciences - Papers (Archive). Retrieved from https://ro.uow.edu.au/hbspapers/3612

Paxinos, G., Xu-Feng, H., Sengul, G., & Watson, C. (2012). Chapter 8—Organization of brainstem nuclei. In J. K. Mai & G. Paxinos (Eds.), *The human nervous system* (3rd ed., pp. 260–327). San Diego, CA: Academic Press. https://doi.org/10.1016/B978-0-12-374236-0.10008-2

Pritchard, T. C. (2012). Chapter 33—Gustatory system. In J. K. Mai & G. Paxinos (Eds.), *The human nervous system* (3rd ed., pp. 1187–1218). San Diego, CA: Academic Press. https://doi.org/10.1016/B978-0-12-374236-0.10033-1

Quessy, S., & Freedman, E. G. (2004). Electrical stimulation of rhesus monkey nucleus reticularis gigantocellularis. I. Characteristics of evoked head movements. *Experimental Brain Research*, *156*(3), 342–356. https://doi.org/10.1007/s00221-003-1787-8

Reisert, M., Weiller, C., & Hosp, J. A. (2021). Displaying the autonomic processing network in humans—A global tractography approach. *NeuroImage*, *231*, 117852. https://doi.org/10.1016/j.neuroimage.2021.117852

Riemann, R., & Reuss, S. (1998). Projection neurons in the superior olivary complex of the rat auditory brainstem: A double retrograde tracing study. *ORL: Journal for Oto-Rhino-Laryngology and its Related Specialties*, *60*(5), 278–282. https://doi.org/10.1159/000027610

Robinson, F. R., Phillips, J. O., & Fuchs, A. F. (1994). Coordination of gaze shifts in primates: Brainstem inputs to neck and extraocular motoneuron pools. *The Journal of Comparative Neurology*, *346*(1), 43–62. https://doi.org/10.1002/cne.903460104

Rubinov, M., & Sporns, O. (2010). Complex network measures of brain connectivity: Uses and interpretations. *NeuroImage*, *52*(3), 1059–1069. https://doi.org/10.1016/j.neuroimage.2009.10.003

Rubinov, M., Sporns, O., van Leeuwen, C., & Breakspear, M. (2009). Symbiotic relationship between brain structure and dynamics. *BMC Neuroscience*, *10*, 55. https://doi.org/10.1186/1471-2202-10-55

Sanvictores, T., & Tadi, P. (2021). Neuroanatomy, autonomic nervous system visceral afferent fibers and pain. In *StatPearls*. Treasure Island, FL: StatPearls Publishing.

Saper, C. B., Chou, T. C., & Scammell, T. E. (2001). The sleep switch: Hypothalamic control of sleep and wakefulness. *Trends in Neurosciences*, *24*(12), 726–731. https://doi.org/10.1016/s0166-2236(00)02002-6

Saper, C. B., Fuller, P. M., Pedersen, N. P., Lu, J., & Scammell, T. E. (2010). Sleep state switching. *Neuron*, *68*(6), 1023–1042. https://doi.org/10.1016/j.neuron.2010.11.032

Saper, C. B., & Loewy, A. D. (1980). Efferent connections of the parabrachial nucleus in the rat. *Brain Research*, *197*(2), 291–317. https://doi.org/10.1016/0006-8993(80)91117-8

Saper, C. B., & Stornetta, R. L. (2015). Central autonomic system. In G. Paxinos (Ed.), *The rat nervous system* (4th ed., pp. 629–673). Oxford, UK: Elsevier. https://doi.org/10.1016/B978-0-12-374245-2.00023-1

Schmidt, R. F. (1989). Integrative functions of the central nervous system. In R. F. Schmidt & G. Thews (Eds.), *Human physiology* (pp. 124–165). Berlin: Springer. https://doi.org/10.1007/978-3-642-73831-9_6

Shammah-Lagnado, S. J., Costa, M. S., & Ricardo, J. A. (1992). Afferent connections of the parvocellular reticular formation: A horseradish peroxidase study in the rat. *Neuroscience*, *50*(2), 403–425. https://doi.org/10.1016/0306-4522(92)90433-3

Shi, X., Wei, H., Chen, Z., Wang, J., Qu, W., Huang, Z., & Dai, C. (2021). Whole-brain monosynaptic inputs and outputs of glutamatergic neurons of the vestibular nuclei complex in mice. *Hearing Research*, *401*, 108159. https://doi.org/10.1016/j.heares.2020.108159

Shinoda, Y., Sugiuchi, Y., Izawa, Y., & Hata, Y. (2006). Long descending motor tract axons and their control of neck and axial muscles. *Progress in Brain Research*, *151*, 527–563. https://doi.org/10.1016/S0079-6123(05)51017-3

Shook, B. L., Schlag-Rey, M., & Schlag, J. (1990). Primate supplementary eye field: I. comparative aspects of mesencephalic and pontine connections. *The Journal of Comparative Neurology*, *301*(4), 618–642. https://doi.org/10.1002/cne.903010410

Sim, L. J., & Joseph, S. A. (1992). Efferent projections of the nucleus raphe magnus. *Brain Research Bulletin*, *28*(5), 679–682. https://doi.org/10.1016/0361-9230(92)90246-t

Singh, K., García-Gomar, M. G., & Bianciardi, M. (2021). Probabilistic atlas of the mesencephalic reticular formation, isthmic reticular formation, microcellular tegmental nucleus, ventral tegmental area nucleus complex, and caudal-rostral linear raphe nucleus complex in living humans from 7 Tesla magnetic resonance imaging. *Brain Connectivity*, *11*(8), 613–623. https://doi.org/10.1089/brain.2020.0975

Singh, K., Indovina, I., Augustinack, J. C., Nestor, K., García-Gomar, M. G., Staab, J. P., & Bianciardi, M. (2019). Probabilistic template of the lateral parabrachial nucleus, medial parabrachial nucleus, vestibular nuclei complex, and medullary viscero-sensory-motor nuclei complex in living humans from 7 Tesla MRI. *Frontiers in Neuroscience*, *13*, 1425. https://doi.org/10.3389/fnins.2019.01425

Snider, S. B., Bodien, Y. G., Bianciardi, M., Brown, E. N., Wu, O., & Edlow, B. L. (2019). Disruption of the ascending arousal network in acute traumatic disorders of consciousness. *Neurology*, *93*(13), e1281–e1287. https://doi.org/10.1212/WNL.0000000000008163

Staab, J. P. (2012). Chronic subjective dizziness. *Continuum*, *18*, 1118–1141. https://doi.org/10.1212/01.CON.0000421622.56525.58

Staab, J. P., Eckhardt-Henn, A., Horii, A., Jacob, R., Strupp, M., Brandt, T., & Bronstein, A. (2017). Diagnostic criteria for persistent postural-perceptual dizziness (PPPD): Consensus document of the committee for the classification of vestibular disorders of the Bárány society. *Journal of Vestibular Research*, *27*(4), 191–208. https://doi.org/10.3233/VES-170622

Staab, J. P., Rohe, D. E., Eggers, S. D. Z., & Shepard, N. T. (2014). Anxious, introverted personality traits in patients with chronic subjective dizziness. *Journal of Psychosomatic Research*, *76*(1), 80–83. https://doi.org/10.1016/j.jpsychores.2013.11.008

Stanton, G. B., Goldberg, M. E., & Bruce, C. J. (1988). Frontal eye field efferents in the macaque monkey: II. Topography of terminal fields in midbrain and pons. *The Journal of Comparative Neurology*, *271*(4), 493–506. https://doi.org/10.1002/cne.902710403

Subramanian, H. H., Huang, Z.-G., Silburn, P. A., Balnave, R. J., & Holstege, G. (2018). The physiological motor patterns produced by neurons in the nucleus retroambiguus in the rat and their modulation by vagal, peripheral chemosensory, and nociceptive stimulation. *The Journal of Comparative Neurology*, *526*(2), 229–242. https://doi.org/10.1002/cne.24318

Sugihara, I., & Shinoda, Y. (2004). Molecular, topographic, and functional organization of the cerebellar cortex: A study with combined aldolase C and olivocerebellar labeling. *The Journal of Neuroscience*, *24*(40), 8771–8785. https://doi.org/10.1523/JNEUROSCI.1961-04.2004

Tache, Y. (2012). Brainstem neuropeptides and vagal protection of the gastric mucosal against injury: Role of prostaglandins, nitric oxide and calcitonin-gene related peptide in capsaicin afferents. *Current Medicinal Chemistry*, *19*(1), 35–42. https://doi.org/10.2174/092986712803414097

Tanaka, M., Okamura, H., Tamada, Y., Nagatsu, I., Tanaka, Y., & Ibata, Y. (1994). Catecholaminergic input to spinally projecting serotonin neurons in the rostral ventromedial medulla oblongata of the rat. *Brain Research Bulletin*, *35*(1), 23–30. https://doi.org/10.1016/0361-9230(94)90211-9

Tang, W., Kochubey, O., Kintscher, M., & Schneggenburger, R. (2020). A VTA to basal amygdala dopamine projection contributes to signal salient somatosensory events during fear learning. *The Journal of Neuroscience*, *40*(20), 3969–3980. https://doi.org/10.1523/JNEUROSCI.1796-19.2020

Tellegen, A. J., Arends, J. J., & Dubbeldam, J. L. (2001). The vestibular nuclei and vestibuloreticular connections in the mallard (*Anas platyrhynchos* L.). an anterograde and retrograde tracing study. *Brain, Behavior and Evolution*, *58*(4), 205–217. https://doi.org/10.1159/000057564

Ter Horst, G. J., Copray, J. C., Liem, R. S., & Van Willigen, J. D. (1991). Projections from the rostral parvocellular reticular formation to pontine and medullary nuclei in the rat: Involvement in autonomic regulation and orofacial motor control. *Neuroscience*, *40*(3), 735–758. https://doi.org/10.1016/0306-4522(91)90009-d

Tournier, J.-D., Calamante, F., & Connelly, A. (2007). Robust determination of the fibre orientation distribution in diffusion MRI: Non-negativity constrained super-resolved spherical deconvolution. *NeuroImage*, *35*(4), 1459–1472. https://doi.org/10.1016/j.neuroimage.2007.02.016

Tournier, J.-D., Calamante, F., & Connelly, A. (2010). Improved probabilistic streamlines tractography by 2nd order integration over fibre orientation distributions. *Proceedings of the International Society for Magnetic Resonance in Medicine*, *18*, 1670.

Tournier, J.-D., Calamante, F., & Connelly, A. (2012). MRtrix: Diffusion tractography in crossing fiber regions. *International Journal of Imaging Systems and Technology*, *22*(1), 53–66.

Tournier, J.-D., Calamante, F., & Connelly, A. (2013). Determination of the appropriate b value and number of gradient directions for high-angular-resolution diffusion-weighted imaging. *NMR in Biomedicine*, *26*(12), 1775–1786. https://doi.org/10.1002/nbm.3017

Uschakov, A., Gong, H., McGinty, D., & Szymusiak, R. (2007). Efferent projections from the median preoptic nucleus to sleep- and arousal-regulatory nuclei in the rat brain. *Neuroscience*, *150*(1), 104–120. https://doi.org/10.1016/j.neuroscience.2007.05.055

Usunoff, K. G., Schmitt, O., Itzev, D. E., Rolfs, A., & Wree, A. (2007). Efferent connections of the parabigeminal nucleus to the amygdala and the superior colliculus in the rat: A double-labeling fluorescent retrograde tracing study. *Brain Research*, *1133*(1), 87–91. https://doi.org/10.1016/j.brainres.2006.11.073

Veening, J. G., Swanson, L. W., & Sawchenko, P. E. (1984). The organization of projections from the central nucleus of the amygdala to brainstem sites involved in central autonomic regulation: A combined retrograde transport-immunohistochemical study. *Brain Research*, *303*(2), 337–357. https://doi.org/10.1016/0006-8993(84)91220-4

Volgin, D. V., Rukhadze, I., & Kubin, L. (2008). Hypoglossal premotor neurons of the intermediate medullary reticular region express cholinergic markers. *Journal of Applied Physiology*, *105*(5), 1576–1584. https://doi.org/10.1152/japplphysiol.90670.2008

Wager, K., & Cox, S. (Eds.) (2009). CHAPTER 6—The limbic (emotional) system. In *Auricular acupuncture & addiction* (pp. 57–67). Philadelphia, USA: Churchill Livingstone. https://doi.org/10.1016/B978-0-443-06885-0.50014-8

Wang, C., Laiwalla, A., Salamon, N., Ellingson, B. M., & Holly, L. T. (2020). Compensatory brainstem functional and structural connectivity in patients with degenerative cervical myelopathy by probabilistic tractography and functional MRI. *Brain Research*, *1749*, 147129. https://doi.org/10.1016/j.brainres.2020.147129

Wang, J., Wang, X., Xia, M., Liao, X., Evans, A., & He, Y. (2015). GRETNA: A graph theoretical network analysis toolbox for imaging connectomics. *Frontiers in Human Neuroscience*, *9*, 386. https://doi.org/10.3389/fnhum.2015.00386

Wang, N., Warren, S., & May, P. J. (2010). The macaque midbrain reticular formation sends side-specific feedback to the superior colliculus. *Experimental Brain Research*, *201*(4), 701–717. https://doi.org/10.1007/s00221-009-2090-0

Webster, D. B. (1992). An overview of mammalian auditory pathways with an emphasis on humans. In D. B. Webster, A. N. Popper, & R. R. Fay (Eds.), *The mammalian auditory pathway: Neuroanatomy* (pp. 1–22). New York, NY: Springer. https://doi.org/10.1007/978-1-4612-4416-5_1

Weissheimer, K. V., & Machado, B. H. (2007). Inhibitory modulation of chemoreflex bradycardia by stimulation of the nucleus raphe obscurus is mediated by 5-HT3 receptors in the NTS of awake rats. *Autonomic Neuroscience*, *132*(1–2), 27–36. https://doi.org/10.1016/j.autneu.2006.09.002

Westlund, K. N., & Willis, W. D. (2012). Chapter 32—Pain system. In J. K. Mai & G. Paxinos (Eds.), *The human nervous system* (3rd ed., pp. 1144–1186). San Diego, CA: Academic Press. https://doi.org/10.1016/B978-0-12-374236-0.10032-X

Wirth, A. M., Frank, S. M., Greenlee, M. W., & Beer, A. L. (2018). White matter connectivity of the visual-vestibular cortex examined by diffusion-weighted imaging. *Brain Connectivity*, *8*(4), 235–244. https://doi.org/10.1089/brain.2017.0544

Wise, R. A. (2004). Dopamine, learning and motivation. *Nature Reviews Neuroscience*, *5*(6), 483–494. https://doi.org/10.1038/nrn1406

Wu, Q., Boyle, M. P., & Palmiter, R. D. (2009). Loss of GABAergic signaling by AgRP neurons to the parabrachial nucleus leads to starvation. *Cell*, *137*(7), 1225–1234. https://doi.org/10.1016/j.cell.2009.04.022

Yamaguchi, T., Wang, H.-L., Li, X., Ng, T. H., & Morales, M. (2011). Mesocorticolimbic glutamatergic pathway. *The Journal of Neuroscience*, *31*(23), 8476–8490. https://doi.org/10.1523/JNEUROSCI.1598-11.2011

Yasui, Y., Saper, C. B., & Cechetto, D. F. (1989). Calcitonin gene-related peptide immunoreactivity in the visceral sensory cortex, thalamus, and related pathways in the rat. *The Journal of Comparative Neurology*, *290*, 487–501. https://doi.org/10.1002/cne.902900404

SUPPORTING INFORMATION

Additional supporting information may be found in the online version of the article at the publisher's website.